2012

Analysis of Swarm Behavior in Two Dimensions

Louis Ryan
Harvey Mudd College

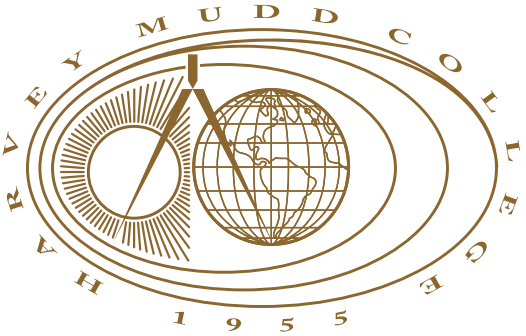

Analysis of Swarm Behavior in Two Dimensions

Louis Ryan

Andrew Bernoff, Advisor

Chad Topaz, Reader

May, 2012

HARVEY MUDD
COLLEGE
Department of Mathematics

Abstract

We investigate the steady state solutions that can exist for a two dimensional swarm of biological organisms, which have pairwise social interaction forces. The three steady states we investigate using a continuum model are a ribbon migrating swarm, a circular migrating swarm, and a milling swarm. We solve these numerically by reformulating the integral equation that arises from the continuum model as an energy minimization problem. For the ribbon migrating solution, we are able to determine an analytic solution from Carleman's equation which arises after an asymptotic expansion of the social interaction potential. Using this technique we are able to show the existence of a square root singularity that emerges at the boundary of the compactly supported swarm. The analytic solution agrees with the numerical solution for certain parameter values in the social interaction potential. We then demonstrate the existence of solutions for a migrating and milling circular swarm which contain a square root singularity. The milling swarm looks similar to the infinite ribbon, so we are able to use an asymptotic expansion of the potential to obtain an analytic solution in this case as well. The singularities in the density of the swarm suggest that the Morse potential should not be used for modeling biological swarming.

Contents

List of Figures

Acknowledgments

I'd like to thank Andrew Bernoff for being an awesome advisor in every way possible and helping me throughout the thesis process. I'd also like to thank Chad Topaz for his support as my second reader and introduction into swarming research over the summer.

Chapter 1

Introduction

Swarming is collective behavior of animals that tend to aggregate. Swarming behavior is observed among a variety of different animals. Two common swarming behaviors are migration and milling. Migration is a well known behavior where the group moves as a whole in a specific direction. Milling is another common swarm behavior where each individual in the group is moving in a circular fashion, so the group as a whole stays in the same place. Swarming is beneficial for groups of animals due to the advantages they gain from social interactions. These can occur from a variety of factors such as the updraft that birds get when flying in a Vee formation which requires the birds to use less energy. In addition to this, swarming is also used as a mechanism for avoiding predation. For example, fish swarms use the fountain effect maneuver where the group splits in two as they move around a predator. In this chapter, we will provide a background into the different types of models used to study swarming behavior.

1.1 Background

There are many models that model the swarming behavior that is observed in biological aggregations. These models fall into two classes, kinematic models where velocity is specified in terms of endogeneous and exogenous social forces and dynamic models where the acceleration is specified. Within these classes, the models can be formulated in two different ways. There are also discrete models which treat each particle as an individual, and continuum models where the particles form a continuous density function. These models attempt to recreate the aligned motion seen in the group

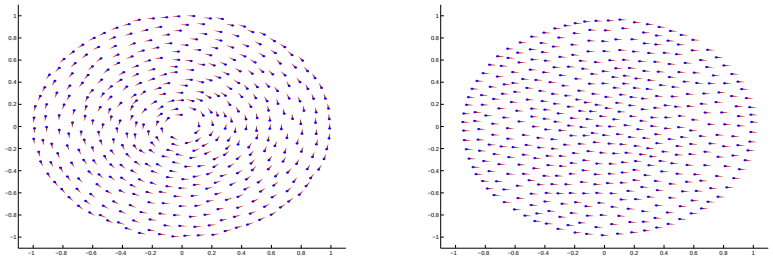

a. Mill **b.** Migration

Figure 1.1 Examples of a swarm exhibiting aligned motion in a mill and migration state.

of individuals.

To model the social interactions between particles, there is a force for long range attraction and short range repulsion. The long range attraction is incorporated since animals are social creatures. These attraction forces exist because it is beneficial for animals to be in groups for mating and predator avoidance (Hamilton, 1971; Hall et al., 1986). Short range repulsion exists to prevent crowding since that leads to competition between individuals over resources (Mogilner et al., 2003).

The area of research in collective behavior is a growing field due to its wide range of applications across the physical sciences. There are direct applications to biology, computer science, engineering, and mathematics. From a biological perspective, the study of collective behavior in animals can provide us with a better understanding of how animals evolve (Couzin and Krause, 2003). In computer science, there are techniques being used such as particle swarm optimization and ant colony optimization that use these social interactions to solve optimization problems. These algorithms work by having candidate solutions (the particles) interact with each other in a manner where particles with good solutions attract other particles. This technique finds a "good" solution for problems which are NP-Complete, meaning that the problem cannot be solved exactly in any reasonable amount of time (Tang et al., 2007). In engineering, the study of collective behavior has been used to create groups of robots that are capable of interacting and working together (Swain et al., 2011).

Figure 1.2 A picture of a school of fish exhibiting swarming behavior. The group of fish have alligned motion and are exhibiting milling behavior (Hannant, 2009).

1.2 Dynamic Models

Dynamical models incorporate the forces felt by particles in the swarm. Whereas a kinematic model describes how the position changes as a function of time, a dynamic model describes how the velocity changes as a function of time. In this paper, we will focus our research on the dynamic model.

1.2.1 The Discrete Model

The model we investigate is based on a paper by Chuang et al. (2007) on self-propelled particle systems. This model was first investigated by Levine et al. (2000). The authors investigate the solutions that exist for a rotating mill state in two dimensions. In the discrete model, movement of each individual is governed by the dimensioned equation

$$m_i \ddot{\mathbf{x}}_i = (\alpha - \beta|\dot{\mathbf{x}}_i|^2)\dot{\mathbf{x}}_i - \nabla_{\mathbf{x}_i} Q_i,$$

where Q_i is the potential

$$Q_i = \sum_{j \neq i} \left(-C_a e^{-\frac{|\mathbf{x}_i - \mathbf{x}_j|}{\ell_a}} + C_r e^{-\frac{|\mathbf{x}_i - \mathbf{x}_j|}{\ell_r}} \right).$$

This is known as the Morse potential, which is the potential function we will be working with for our model. Below is a description of the parameters used in this model.

α	:	determines the self propelling force in the model
β	:	provides the drag force in the model
ℓ_a	:	length of attraction scale between particles
ℓ_r	:	length of repulsion scale between particles
C_a	:	amplitude of the attraction between particles
C_a	:	amplitude of the repulsion between particles
m_i	:	mass of the i^{th} particle in the swarm

In order for the Morse potential to have long range attraction we require that the length scale $\ell_a > \ell_r$. We nondimensionalized the potential above to

$$Q(z) = e^{-|z|} - Ce^{-|z|/L},$$

where $C = C_a/C_r$ and $L = \ell_a/\ell_r$. We will use this nondimensionalized potential to investigate the model. Since we want $\ell_a > \ell_r$, we are interested in behaviors for $L > 1$.

1.2.2 The Continuum Model

The continuum model is derived by considering the limit as the number of particles $N \to \infty$. The formulation of this model is derived in Chuang et al. (2007) which leads to the following equations:

$$\begin{aligned}
\rho_t + \nabla \cdot (\mathbf{v}\rho) =& 0, \\
\mathbf{v}_t + (\mathbf{v} \cdot \nabla)\mathbf{v} =& \alpha\mathbf{v} - \beta|\mathbf{v}|\mathbf{v} - \frac{1}{m^2}\int \nabla Q\left(|\mathbf{x} - \mathbf{x}'|\right)\rho(\mathbf{x})\mathrm{d}x'.
\end{aligned}$$

Here, m represents the mass of an individual particle. We will choose the mass of the individual particle to be 1 which simplifies the equations to

$$\begin{aligned}
\rho_t + \nabla \cdot (\mathbf{v}\rho) =& 0, \\
\mathbf{v}_t + (\mathbf{v} \cdot \nabla)\mathbf{v} =& \alpha\mathbf{v} - \beta|\mathbf{v}|\mathbf{v} - \int \nabla Q\left(|\mathbf{x} - \mathbf{x}'|\right)\rho(\mathbf{x})\mathrm{d}x'.
\end{aligned}$$

The first equation here reflects the conservation of mass while the second reflects the change in velocity that follows the discrete model. This model is useful to determine the steady state behavior of the swarms, so we will use this model to perform our analysis.

1.3 Kinematic Models

Kinematic models study how the movement of the particles changes over time, without an inclusion of the acceleration due to forces. This class of models has been investigated in Leverentz et al. (2009) and Bernoff and Topaz (2011). In the continuum model, the equations governing the motion are given in Bernoff and Topaz (2011) by

$$\rho_t + (\rho v)_x = 0,$$
$$v = \int_{-\infty}^{\infty} q(x-y)\rho(y)dy + f(x).$$

The first equation represents the conservation of mass for the continuum density ρ. The second equation represents the social interactions felt by the particle in addition to an exogenous force $f(x)$. In this model $q(x-y) = -\nabla Q$ represents the effect of social interactions, which is a function of the distance between the particles. These equations are derived from the analogous discrete model,

$$\frac{dx_i}{dt} = V_i(x_1, \ldots, x_n),$$
$$V_i(x_1, \ldots, x_n) = \sum_{j \neq i} mq(x_i - x_j) + f(x_i),$$

where x_i represents the location of the i^{th} particle in the swarm, V_i represents the velocity of the i^{th} particle, and $f(x_i)$ is the exogenous force exerted by the i^{th} particle.

This class of models has been used to model the behavior of locust swarms. These locust swarms can be destructive when they travel in a rolling motion due to the force by the wind. These solutions have been shown to exist in the kinematic model in the presence of an exogenous force. Other solutions have also been shown to exist involving solutions that spread asymptotically, contract to a single location, or go to a compact steady state (Leverentz et al., 2009). We will refer to swarms that contract to a single location as attractive swarms.

1.4 Literature Review

Previous work by Leverentz, Topaz, and Bernoff (2009) examined ways to predict the qualitative behavior of a swarm for the kinematic model. They showed that knowing the first moment of the social interaction kernel and

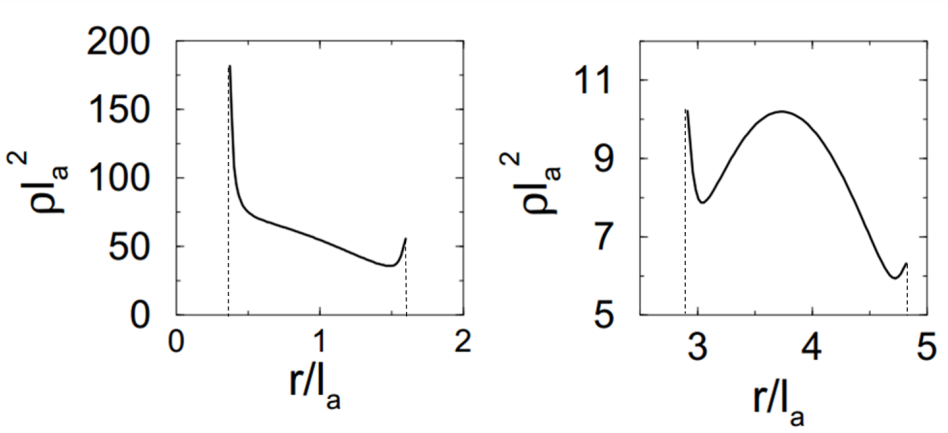

Figure 1.3 The swarm density obtained numerically from the paper by Levine et al. (2000).

the limiting behavior of the origin were sufficient to determine the long term behavior of the swarm.

There is an alternative model constructed by Couzin, Krause, James, Ruxton, and Franks (2002) which incorporates a zone of attraction, a zone of repulsion, and a zone of orientation. In the zone of orientation, there is an alignment term which states that particles at a certain distance prefer to align with each other. This model also exhibits the migration and milling solutions observed in our model.

A similar model to ours was investigated in 2000 by Levine, Rappel, and Cohen in constructing the continuum solution. They observed increases in the swarm density near the boundary of the support. A diagram illustrating one of their solutions is shown in Figure 1.3.

This increase in the swarm density near the boundary resembles an unresolved singularity. We observe the phenomenon in our model results and are able to classify it as a square root singularity.

Bernoff and Topaz (2011) demonstrated that there cannot be a δ concentration located in the interior of a domain. In our study of the dynamic model, we find a solution whose density diverges. However, it does not violate the above condition since the singularity observed is a square root singularity on the boundary.

Chapter 2

Steady States

When investigating swarms, one aspect of interest is the long term behavior of the swarm. We are interested in three different steady states that arise from this model. The first one is a migration solution along a ribbon. This is an infinite swarm that is moving with a constant velocity in a direction parallel to the ribbon. The second steady state solution we are interested in is a circular swarm that is also migrating with a constant velocity. Our last steady state of interest is a milling solution. This corresponds to a solution with a constant velocity that is rotating in a circle. Since the angular velocity is not constant, this is different from rigid body rotation. In this section, we derive the integral equation that arises out of the continuum model, which allows us to solve for the density function ρ.

2.1 Migration on a Ribbon

For a migrating swarm along a ribbon, we are working under the ansatz that the density will only be a function of its relative height (y-position) in the swarm and that the velocity will be constant. For this solution, we are solving on the domain $\Omega = (-\infty, \infty) \times [-\ell, \ell]$. Mathematically this implies $\rho = \bar{\rho}(y)$ and $\mathbf{v} = \bar{v}\hat{\mathbf{x}}$. A diagram of this ansatz is shown in Figure 2.1.

We substitute this ansatz into the governing equations for the continuum model below:

$$\begin{aligned}
&\rho_t + \nabla \cdot (\mathbf{v}\rho) = 0, \\
&\mathbf{v}_t + (\mathbf{v} \cdot \nabla)\mathbf{v} = \alpha\mathbf{v} - \beta|\mathbf{v}|\mathbf{v} - \int \nabla Q\left(\mathbf{x} - \mathbf{x}'\right) \rho(\mathbf{x}) \mathrm{d}x'.
\end{aligned}$$

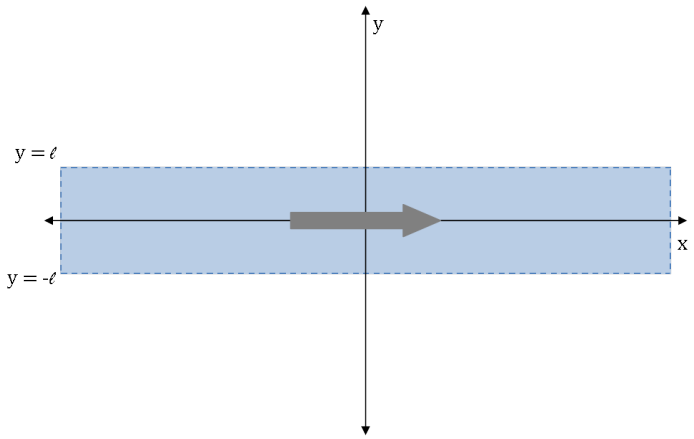

Figure 2.1 A diagram of the ribbon steady state solution.

First we evaluate the left-hand side of the conservation of mass equation. Since the velocity is constant and ρ is not changing in time, this gives

$$\rho_t + \nabla \cdot (\mathbf{v}\rho) = \nabla \cdot (\bar{v}\bar{\rho}(y)\hat{x}) = 0.$$

The conservation of mass equation is satisfied under this ansatz since the density ρ isn't changing in time, and the density is a function in an orthogonal direction to the motion of the swarm. Next, we evaluate the left-hand side of the equation of motion for the migrating swarm. Substituting the ansatz into this equation gives

$$\mathbf{v}_t + (\mathbf{v} \cdot \nabla)\mathbf{v} = (\bar{v}\frac{\partial}{\partial x})\bar{v}\hat{\mathbf{x}} = 0.$$

We define the convolution as

$$\rho * Q \equiv \int Q\left(|\mathbf{x} - \mathbf{x}'|\right)\rho(\mathbf{x})\mathrm{d}x'.$$

Now we evaluate the right-hand side of the equation of motion for the migrating swarm which gives

$$\begin{aligned}\alpha\mathbf{v} - \beta|\mathbf{v}|\mathbf{v} - \int \nabla Q\left(|\mathbf{x} - \mathbf{x}'|\right)\rho(\mathbf{x})\mathrm{d}x' &= (\alpha - \beta\bar{v}^2)\bar{v}\hat{\mathbf{x}} - \int \nabla Q\left(|\mathbf{x} - \mathbf{x}'|\right)\rho(\mathbf{x})\mathrm{d}x', \\ &= (\alpha - \beta\bar{v}^2)\bar{v}\hat{\mathbf{x}} - \nabla(\rho * Q).\end{aligned}$$

This follows from the property of the convolution $\nabla(\rho * Q) = (\nabla\rho) * Q$. We equate this with the result from above which gives

$$0 = (\alpha - \beta\bar{v}^2)\bar{v}\hat{\mathbf{x}} - \nabla\rho * Q.$$

This gives the following two equations:

$$0 = (\alpha - \beta\bar{v}^2)\bar{v} - \frac{\partial}{\partial x}\rho * Q,$$
$$0 = \frac{\partial}{\partial y}\rho * Q.$$

If we write out the convolution $\rho * Q$ we see that

$$\rho * Q = \int_{x'=-\infty}^{\infty}\int_{y'=-\infty}^{\infty}\rho(y')Q\left(\sqrt{(x-x')^2 + (y-y')^2}\right)\mathrm{d}y'\mathrm{d}x'.$$

If we let $z = x - x'$ this becomes

$$\rho * Q = \int_{z=-\infty}^{\infty}\int_{y'=-\infty}^{\infty}\rho(y')Q\left(\sqrt{z^2 + (y-y')^2}\right)\mathrm{d}y'\mathrm{d}z = \Lambda(y).$$

This implies that

$$\frac{\partial}{\partial x}\rho * Q = 0,$$

which implies

$$(\alpha - \beta\bar{v})\bar{v} = 0.$$

Therefore, we know that the steady state velocity will be $\bar{v} = \sqrt{\frac{\alpha}{\beta}}$. Substituting this back into the equations gives

$$0 = \frac{\partial}{\partial x}\rho * Q,$$
$$0 = \frac{\partial}{\partial y}\rho * Q.$$

Together, these two equations imply that on a migrating ribbon

$$\rho * Q = \lambda \in \Omega.$$

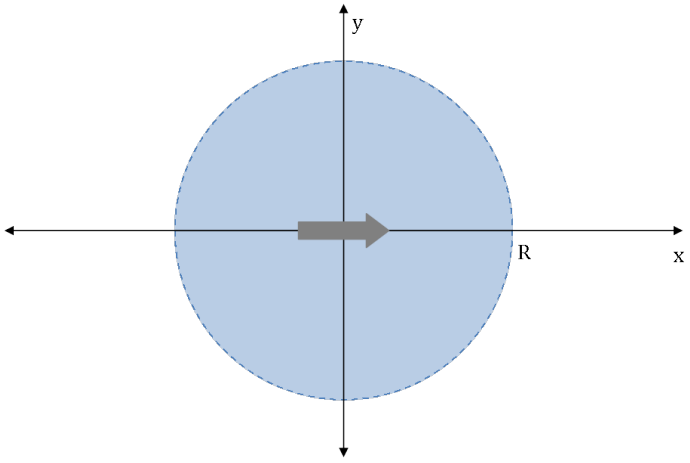

Figure 2.2 A diagram of the circular steady state solution.

2.2 Circular Swarm Migration

We can perform a similar analysis for a migrating circular swarm. For a migrating circular swarm, the velocity will be constant, $\mathbf{v} = \bar{v}\hat{\mathbf{x}}$, and the density will only be a function of the radius in the moving frame. A diagram of this ansatz is shown in Figure 2.2.

In the moving frame we use the change of variables,

$$\begin{aligned}\xi &= x - \bar{v}t,\\ \eta &= y.\end{aligned}$$

Thus our steady state solution becomes $\rho = \bar{\rho}(r)$ where $r = \sqrt{\xi^2 + \eta^2}$ and $\mathbf{v} = \mathbf{v}(\xi, \eta) = \mathbf{0}$. Substituting this ansatz into the conservation of mass equation gives

$$-\bar{v}\rho_\xi + \nabla \cdot (\mathbf{v}\rho) = -\bar{v}\rho_\xi + \bar{v}\rho_\xi = 0.$$

This follows since the density isn't changing in time. Similarly, for the equations of motion we get

$$\begin{aligned}\mathbf{v}_t + (\mathbf{v}\cdot\nabla)\mathbf{v} &= -\bar{v}\mathbf{v}_\xi + (\mathbf{v}\cdot\nabla_\xi + \bar{v}\frac{\partial}{\partial\xi})\mathbf{v},\\ &= (\mathbf{v}\cdot\nabla_\xi)\mathbf{v} = \mathbf{0}.\end{aligned}$$

Now evaluating the right-hand side in our original reference frame yields

$$\alpha\mathbf{v} - \beta|\mathbf{v}|\mathbf{v} - \int \nabla Q\left(|\mathbf{x}-\mathbf{x}'|\right)\rho(\mathbf{x})\mathrm{d}x' = (\alpha - \beta\bar{v}^2)\bar{v}\hat{\mathbf{x}} - \int \nabla Q\left(|\mathbf{x}-\mathbf{x}'|\right)\rho(\mathbf{x})\mathrm{d}x',$$
$$0 = (\alpha - \beta\bar{v}^2)\bar{v}\hat{\mathbf{x}} - \nabla\rho * Q.$$

This yields the same two equations as in the ribbon case,

$$0 = (\alpha - \beta\bar{v}^2)\bar{v} - \frac{\partial}{\partial x}\rho * Q$$
$$0 = \frac{\partial}{\partial y}\rho * Q.$$

Since ρ only depends on r, by symmetry we get that $\rho * Q$ is a function of r. If we integrate both sides of the first equation from $x = -L$ to L, we get

$$(\alpha - \beta\bar{v}^2)\bar{v} = \rho * Q\Big|_{-\ell}^{\ell} = 0.$$

Thus, the steady state velocity will still be $\bar{v} = \sqrt{\frac{\alpha}{\beta}}$, so for a circular migrating swarm,

$$\rho * Q = \lambda \in \Omega.$$

Here, we note that the domain $\Omega = r \in [0, R], \theta \in [0, 2\pi]$ is different since we are solving the integral equation over a circular domain.

2.3 Milling Swarm

For a milling steady state, we are looking to find solutions under the ansatz that the potential function and the density function only depend on radius, and that the velocity is in the $\hat{\theta}$ so we have a rotating solution. This means that $Q = Q(r)$, $\rho = \rho(r)$, and $\mathbf{v} = \bar{v}\hat{\theta}$. A diagram of this ansatz is shown in Figure 2.3.

We substitute this ansatz into the governing equations,

$$\rho_t + \nabla\cdot(\mathbf{v}\rho) = 0,$$
$$\mathbf{v}_t + (\mathbf{v}\cdot\nabla)\mathbf{v} = \alpha\mathbf{v} - \beta|\mathbf{v}|\mathbf{v} - \int \nabla Q\left(|\mathbf{x}-\mathbf{x}'|\right)\rho(\mathbf{x})\mathrm{d}x'.$$

When we evaluate the conservation of mass equation, we see

$$\rho_t + \nabla\cdot(\mathbf{v}\rho) = \rho(y)_t + \bar{v}\nabla\cdot\rho(r)\hat{\theta},$$
$$\rho_t + \nabla\cdot(\mathbf{v}\rho) = 0 + \bar{v}\cdot 0 = 0.$$

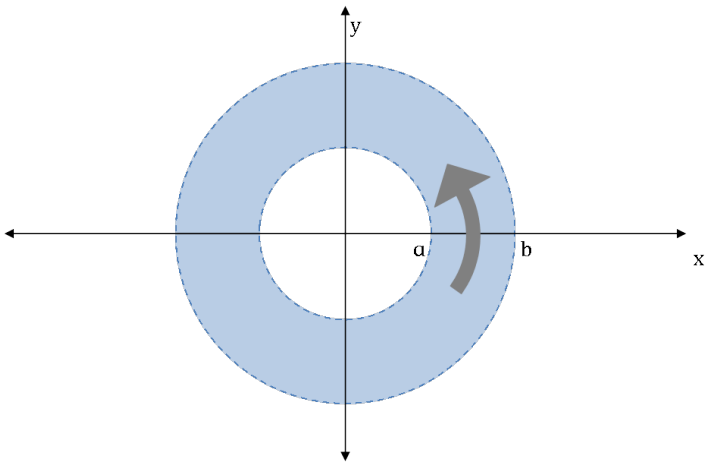

Figure 2.3 A diagram of the milling steady state solution.

Thus, the conservation of mass equation remains satisfied under these assumptions. Next, we evaluate the equations of motion,

$$\begin{aligned}\mathbf{v}_t &= 0,\\ (\mathbf{v}\cdot\nabla) &= \bar{v}\frac{1}{r}\frac{d}{d\theta},\\ (\mathbf{v}\cdot\nabla)\mathbf{v} &= \bar{v}^2\frac{1}{r}(-\hat{r}).\end{aligned}$$

This simplifies the equation of motion to

$$(\alpha-\beta|\mathbf{v}|^2)\mathbf{v}-\nabla\rho*Q=-\bar{v}^2\frac{1}{r}\hat{r}.$$

Next, we can break this up into the radial and angular components. Since $\rho*Q$ is radial this implies that $\nabla\rightarrow\hat{r}\frac{d}{dr}$ because the θ component vanishes. Thus, we get the two equations

$$\begin{aligned}\text{Angular:}\quad & (\alpha-\beta\bar{v}^2)\bar{v}=0.\\ \text{Radial:}\quad & -\frac{\partial}{\partial r}\rho*Q=-\bar{v}\frac{1}{r}.\end{aligned}$$

For both of these to be satisfied we must have $\bar{v}=\sqrt{\frac{\alpha}{\beta}}$ so the velocity is

$$\mathbf{v}=\sqrt{\frac{\alpha}{\beta}}\hat{\theta}.$$

We can substitute this velocity into the radial equation which gives

$$-\frac{\partial}{\partial r}\rho * Q = -\sqrt{\frac{\alpha}{\beta}}\frac{1}{r}.$$

Now we can integrate both sides of the radial equation which gives

$$\frac{\alpha}{\beta}\ln r + \lambda = \rho * Q \in \Omega.$$

This provides the integral equation that is satisfied for the milling solution.
Here we are also working on a circular domain $\Omega = [a, b] \times [0, 2\pi]$.

Chapter 3

Ribbon Solution

In this section we will investigate the ribbon steady state solution. The ribbon solution is when a swarm is migrating in a specific direction on a ribbon, or more formally on the domain $\Omega = (-\infty, \infty) \times [-\ell, \ell]$. In Section 2.1 we showed that a ribbon has the steady state solution $\rho = \rho(y), \mathbf{v} = \sqrt{\frac{\alpha}{\beta}}\hat{\mathbf{x}}$. This led to the following integral equation:

$$\int_\Omega p(\mathbf{x}')Q(|\mathbf{x} - \mathbf{x}'|)\mathrm{d}\mathbf{x}' = \lambda.$$

3.1 Reducing the Dimension

The integral equation we are solving is currently a two-dimensional integral equation. We can reduce this to a one-dimensional integral equation by letting

$$Q_{2D}(|y' - y|) = \int_{-\infty}^{\infty} Q(|\mathbf{x} - \mathbf{x}'|)\mathrm{d}x.$$

Following Bernoff and Topaz (2011), we let $s = x' - x$ and $z = y' - y$, which simplifies the above equation to

$$Q_{2D}(z) = \int_{-\infty}^{\infty} Q(\sqrt{s^2 + z^2})\mathrm{d}s = 2\int_0^{\infty} Q(\sqrt{s^2 + z^2})\mathrm{d}s.$$

From Bernoff and Topaz, we see that we can evaluate the integral Q_{2D} using a finite domain by using the substitution $s = z\tan\theta$ so $\mathrm{d}s = z\sec^2\theta\mathrm{d}\theta$. This gives the integral

$$\tilde{Q}_{2D}(z) = 2|z|\int_0^{\pi/2} e^{-|z|\sec\theta}\sec^2\theta\,\mathrm{d}\theta.$$

This provides the value $\tilde{Q}_{2D}$ for Laplace's potential which only includes repulsion. The nondimensionalized Morse potential is given by

$$Q(z) = e^{-|z|} - Ce^{-|z|/L}.$$

Thus, we can compute the two-dimensional potential

$$Q_{2D}(z) = \tilde{Q}_{2D}(z) - C\tilde{Q}_{2D}\left(\frac{z}{L}\right).$$

Using this formulation leads a one-dimensional integral equation,

$$\int_{-\ell}^{\ell} \rho(y')Q_{2D}(|y-y'|)\mathrm{d}y' = \lambda \in \Omega.$$

This can be solved by discretizing the domain $[-\ell, \ell]$ with points $y_0, y_1, \ldots, y_n$ and evaluating $Q_{2D}(z)$ for different distances $|y_i - y_j|$.

3.2 Numerical Solution

To solve the integral equation numerically, we start by letting

$$\rho = \sum_i m_i \delta(x - x_i),$$

and define the energy to be

$$W = \frac{1}{2}\sum_{i,j} m_i m_j Q_{2D}(|\mathbf{x_i} - \mathbf{x_j}|).$$

The numerical result is obtained by minimizing this energy. A minimum to the energy will be a solution to the discretized ribbon. This is seen by taking the derivative of the energy with respect to m_i,

$$\frac{dW}{dm_i} = \sum_j m_j Q_{2D}(|\mathbf{x_i} - \mathbf{x_j}|).$$

Next, we solve this numerically using Matlab's `fmincon` method in the optimization toolbox. The interior-point algorithm was selected to perform the minimization. The tolerance for the objective function and the constraints was set to 10^{-15}. A center of mass constraint was added to the problem to ensure that that any attractive swarm would be located at the origin. There was a total mass constraint that $\sum_i \rho(x_i) = M$ and for all

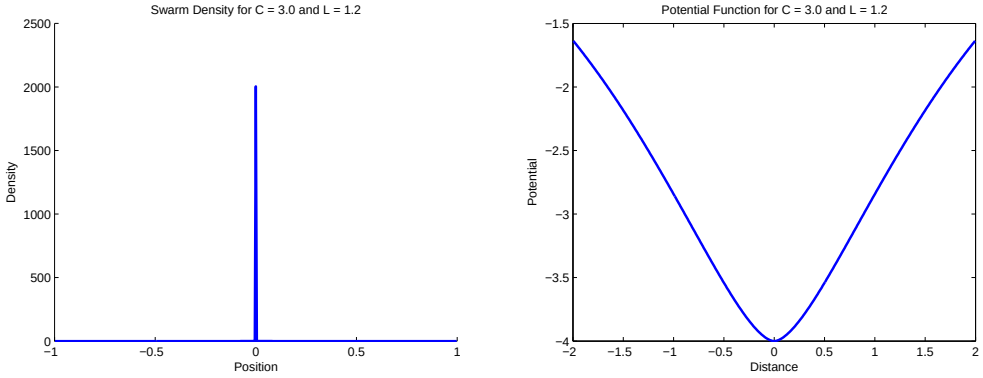

Figure 3.1 The swarm density and the corresponding potential function for an attractive swarm with a delta function at the origin.

points in the interval $\rho(x_i) \geq 0$. The gradient and the Hessian were supplied to the optimization. The Hessian is computed below:

$$\frac{d^2W}{dm_i dm_j} = Q_{2D}(|\mathbf{x_i} - \mathbf{x_j}|).$$

Using this framework, we can numerically solve for the swarm density using the Morse potential. The behavior of the swarm is altered based on the choice for the relative length scale L, and relative strength of attraction C. In order for this social interaction potential to be realistic, we only consider the case when $L > 1$ since this corresponds to attraction at longer length scales. When varying the parameters for C, L, we observe 3 different types of density function for the swarm. The results are shown in Figures 3.1, 3.2, and 3.3.

For the compactly supported swarm, we notice that the swarm density has a square root singularity. This suggests that Carleman's equation might be involved in the solution, which we investigate in Section 3.4.

3.3 Swarm Behavior

The behavior of the swarm can be characterized as attractive, spreading, or a compact swarm. The Fourier transform is used to determine the parameter region where a spreading swarm exists. A spreading solution exists when the Fourier transform,$\hat{Q}_{2D}(k)$, is positive definite. It is sufficient to

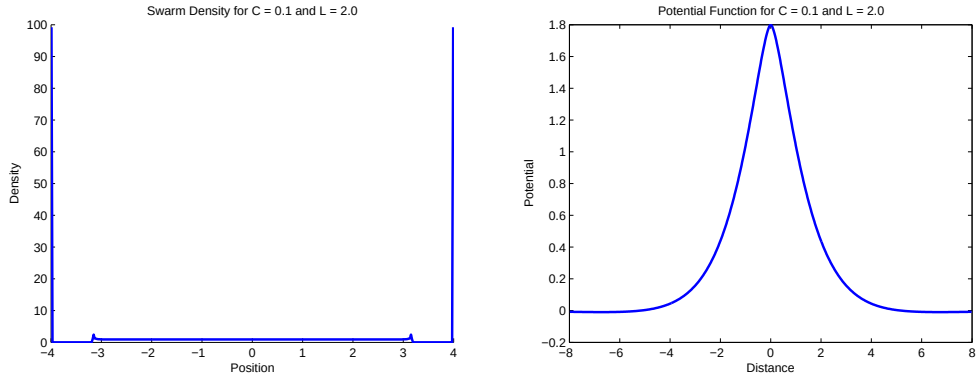

Figure 3.2 The swarm density and the corresponding potential function for a spreading swarm which spreads off to infinity. Here, we get two delta functions on the boundary of the domain we are minimizing the energy on since the mass wants to spread.

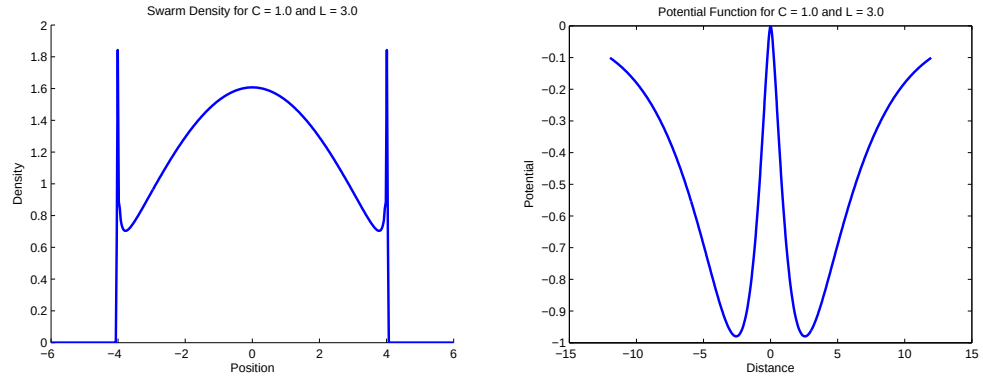

Figure 3.3 The swarm density and the corresponding potential function for a swarm with compact support. This solution has square root singularities at the boundaries of its support.

check that the value of $\hat{Q}_{2D}(k)$ at $k = 0$ and $k = \infty$ are both positive since the function is monotonic (Bernoff and Topaz, 2011). We will define the function

$$F_{2D}(z) = \int_{s=-\infty}^{\infty} e^{-\sqrt{s^2+z^2}} ds.$$

From Bernoff and Topaz (2011), we can express the social interaction potential for the ribbon as

$$Q_{2D}(x) = F_{2D}(x) - CF_{2D}\left(\frac{x}{L}\right).$$

In order to compute the Fourier transform for this, we start by evaluating the Fourier transform for F_{2D}:

$$\begin{aligned} F_{2D}(z) &= 2|z| \int_{s=0}^{\infty} e^{-|z|\sqrt{1+s^2}} ds, \\ \hat{F}_{2D}(k) &= \int_{z=-\infty}^{\infty} F_{2D}(z) e^{-ikz} dz, \\ &= \int_{s=0}^{\infty} \int_{z=-\infty}^{\infty} 2|z| e^{-|z|\sqrt{1+s^2}} e^{-ikz} dz ds. \end{aligned}$$

This gives that the inner integral evaluates to

$$\int_{z=-\infty}^{\infty} 2|z| e^{-|z|\sqrt{1+s^2}} e^{-ikz} dz = \frac{4(1+s^2-k^2)}{(k^2+(1+s^2))^2}.$$

Now we substitute this back into the original equation,

$$\begin{aligned} \hat{F}_{2D}(k) &= \int_{s=0}^{\infty} \frac{4(1+s^2-k^2)}{(k^2+(1+s^2))^2} ds, \\ \hat{F}_{2D}(k) &= \frac{2\pi}{(1+k^2)^{\frac{3}{2}}}. \end{aligned}$$

This result allows us to compute the Fourier transform for the Morse potential with attraction and repulsion,

$$\hat{Q}_{2D}(k) = \hat{F}_{2D}(k) - C\hat{F}_{2D}\left(\frac{k}{L}\right).$$

We substitute the result for the Fourier transform $\hat{F}_{2D}$, which yields

$$\hat{Q}_{2D}(k) = \frac{2\pi}{(1+k^2)^{\frac{3}{2}}} - CL\frac{2\pi}{[1+(kL)^2]^{\frac{3}{2}}}.$$

Then, we evaluate this Fourier transform at k = 0 to find the condition for when $\hat{Q}_{2D}(0) > 0$. This gives

$$\hat{Q}_{2D}(0) = 2\pi - 2\pi\frac{C}{L} > 0,$$

which implies that $C < \frac{1}{L}$. Next, we evaluate $\hat{Q}_{2D}(k)$ in the limit $k \to \infty$,

$$\lim_{k\to\infty} \hat{Q}_{2D}(k) = \lim_{k\to\infty} 2\pi\frac{1}{k^3}\left(1 - \frac{C}{L^2}\right) > 0.$$

This limit implies that $C < L^2$. In order to have a realistic social interaction potential, the length scale $L > 1$. The condition $C < \frac{1}{L}$ implies the condition $C < L^2$, so we only need the condition $C < \frac{1}{L}$ for a spreading solution. In order to have a purely attractive swarm, the potential must reach a minimum at the origin. This can be evaluated using an asymptotic expansion of the potential. We show in Section 3.5 that the asymptotic expansion of the potential is given by

$$Q_{2D}(z) = Bz^2 \ln|ze^{\frac{A}{B}}|,$$

where $A = (1 - \frac{C}{L^2})(\gamma - \frac{1}{2} - \ln 2) + \frac{C}{L^2}\ln|L|$ and $B = (1 - \frac{C}{L^2})$. The function $z^2 \ln|z|$ obtains a local maximum at $z = 0$, so $z^2 \ln|ze^{\frac{A}{B}}|$ will also obtain a local maximum at the origin. In order for $Q_{2D}(z)$ to be a minimum at the origin, the constant B must be less than 0 to flip the sign of the function $z^2 \ln|ze^{\frac{A}{B}}|$. Therefore, we know that for

$$1 - \frac{C}{L^2} < 0,$$

or $L^2 < C$ implies an attractive swarm that will form a delta function.

If neither of these two conditions are met, then there will be a swarm with compact support. To determine if the numerical and predicted results for the swarm density match, a test over the parameter space is run. The swarm is classified as attractive if at least 95% of the mass lies at the center point. It is classified as a spreading swarm if at least 95% of the total mass lies on the boundaries. If neither of these conditions are met, then the swarm will be classified as having compact support if at least 90% of its total mass lies on the interior. Otherwise, the swarm is labeled ambiguous if none of the conditions are satisfied. As seen in Figure 3.4, the observed behavior from the numerical simulations matches with the predicted swarm behavior.

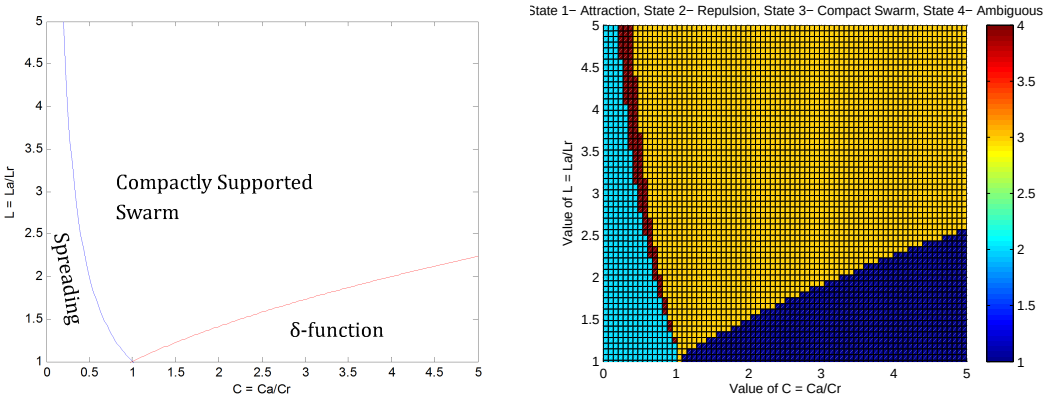

a. Analytic **b.** Numeric

Figure 3.4 A diagram describing the different regions of swarm behaviors over a range of parameter values for C and L. On the left is the analytic prediction for the regions and on the right is the numerical solution.

3.4 Carleman's Equation

For the Ribbon solution, we are solving the equation $\rho * Q = \lambda$. Since the asymptotic expansion of the potential has the form $Q(z) = z^2 \log|z|$, we try to solve the integral equation for this potential. We start by taking two derivatives of the potential,

$$Q''(z) = 2\log|z| + 3.$$

Taking two derivatives of both sides of the equation above yields

$$\begin{aligned}
\frac{d^2}{dy^2}\int_{-\ell}^{\ell}\rho(y')Q(y-y')\mathrm{d}y' &= \frac{d^2}{dy^2}\lambda,\\
\int_{-\ell}^{\ell}\rho(y')Q''(y-y')\mathrm{d}y' &= 0,\\
\int_{-\ell}^{\ell}\rho(y')(2\log|y'-y|+3)\mathrm{d}y' &= 0,\\
2\int_{-\ell}^{\ell}\rho(y')\log|y'-y|\mathrm{d}y' + 3\int_{-\ell}^{\ell}\rho(y)\mathrm{d}y' &= 0,\\
2\int_{-\ell}^{\ell}\rho(y')\log|y'-y|\mathrm{d}y' + 3M &= 0,
\end{aligned}$$

$$\int_{-\ell}^{\ell} \rho(y') \log|y' - y| \mathrm{d}y' = -\frac{3M}{2}.$$

This is Carleman's equation, which has solution $\rho(y) = \dfrac{c}{\sqrt{\ell^2 - y^2}}$ for some constant c. The constant c is obtained by integrating the mass,

$$\begin{aligned} M &= \int_{-\ell}^{\ell} \rho(y) \mathrm{d}y, \\ &= \int_{-\ell}^{\ell} \frac{c}{\sqrt{L^2 - y^2}} \mathrm{d}y, \\ &= c\pi, \\ c &= \frac{M}{\pi}. \end{aligned}$$

Next, we need to find the length of the interval. This is done by evaluating the integral $I = \int_{-\ell}^{\ell} \rho(y) \log|y - y'| \mathrm{d}y'$,

$$\begin{aligned} I &= \int_{-\ell}^{\ell} \rho(y) \log|y - y'| \mathrm{d}y', \\ &= \int_{-\ell}^{\ell} \frac{c}{\sqrt{\ell^2 - y'^2}} \log|y' - y| \mathrm{d}y', \\ &= c \int_{-1}^{1} \frac{\log\left(L|z - w|\right)}{\sqrt{1 - z^2}} \mathrm{d}z, \end{aligned}$$

which follows from the substitution $z = \frac{y'}{L}$ and $w = \frac{y}{L}$. Next we use the trig substitution $z = \sin\theta$ and $w = \sin\phi$ which gives

$$\begin{aligned} I &= c \int_{-\frac{\pi}{2}}^{\frac{\pi}{2}} \frac{\log\left(L|\sin\theta - \sin\phi|\right)\cos\theta}{\cos\theta} \mathrm{d}\theta, \\ \frac{I}{c} &= \pi \log\ell + \int_{-\frac{\pi}{2}}^{\frac{\pi}{2}} \log|\sin\theta - \sin\phi| \mathrm{d}\theta, \\ &= \pi \log\ell + \int_{-\frac{\pi}{2}}^{\frac{\pi}{2}} \log\left|2\cos\frac{\theta + \phi}{2} \sin\frac{\theta - \phi}{2}\right| \mathrm{d}\theta, \\ &= \pi \log\ell + \pi\log 2 + \int_{-\frac{\pi}{2}}^{\frac{\pi}{2}} \log\left|\cos\frac{\theta + \phi}{2}\right| \mathrm{d}\theta + \int_{-\frac{\pi}{2}}^{\frac{\pi}{2}} \log\left|\sin\frac{\theta - \phi}{2}\right| \mathrm{d}\theta. \end{aligned}$$

Using the substitution $u = \frac{\theta+\phi}{2}$ and $v = \frac{\pi-\theta+\phi}{2}$, we get

$$\begin{aligned}
\frac{I}{c} &= \pi \log \ell + \pi \log 2 + 2 \int_{-\frac{\pi}{4}+\frac{\phi}{2}}^{\frac{\pi}{4}+\frac{\phi}{2}} \log|\cos u| \mathrm{d}u - 2 \int_{\frac{3\pi}{4}+\frac{\phi}{2}}^{\frac{\pi}{4}+\frac{\phi}{2}} \log|\cos v| \mathrm{d}v, \\
&= \pi \log \ell + \pi \log 2 + 2 \left(\int_{-\frac{\pi}{4}+\frac{\phi}{2}}^{\frac{\pi}{4}+\frac{\phi}{2}} \log|\cos u| \mathrm{d}u + \int_{\frac{\pi}{4}+\frac{\phi}{2}}^{\frac{3\pi}{4}+\frac{\phi}{2}} \log|\cos v| \mathrm{d}v \right), \\
&= \pi \log \ell + \pi \log 2 + 2 \int_{-\frac{\pi}{4}+\frac{\phi}{2}}^{\frac{3\pi}{4}+\frac{\phi}{2}} \log|\cos u| \mathrm{d}u.
\end{aligned}$$

Since this function is periodic, this simply becomes

$$\begin{aligned}
\frac{I}{c} &= \pi \log \ell + \pi \log 2 + 2 \int_{-\frac{\pi}{4}}^{\frac{3\pi}{4}} \log|\cos u| \mathrm{d}u, \\
&= \pi \log \ell - \pi \log 2.
\end{aligned}$$

Next, we equate this with the result $I = \frac{-3M}{2}$, which gives

$$\begin{aligned}
\frac{I}{c} &= \pi \log \ell - \pi \log 2, \\
\pi \frac{-3}{2} &= \pi \log \ell - \pi \log 2, \\
\log \ell &= \frac{-3}{2} + \log 2, \\
\ell &= 2e^{\frac{-3}{2}}.
\end{aligned}$$

This gives us the length scale of our interval. We know ρ was a solution for

$$\int_{-\ell}^{\ell} \rho(y') Q''(y - y') \mathrm{d}y' = 0,$$

and this will also be a solution for

$$J = \int_{-\ell}^{\ell} \rho(y') Q(y - y') \mathrm{d}y' = \lambda.$$

This follows since the general form of $J = \lambda + by^2$, because the integrand is an even function here. We chose the length scale such that $b = 0$. Thus we can find the value for λ by evaluating the integral when $y = 0$. This gives $\lambda = \int_{-\ell}^{\ell} \rho(y) Q(y) \mathrm{d}y$, which is

$$\lambda = \int_{-\ell}^{\ell} \frac{M}{\pi} \frac{1}{\sqrt{L^2 - y^2}} y^2 \log|y| \mathrm{d}y = \frac{1}{4} L^2 M (1 + \log \frac{L^2}{4}).$$

Putting everything together gives us the overall solution to the equation, which is

$$\rho(y) = \frac{M}{\pi\sqrt{4e^{-3} - y^2}}.$$

3.5 Asymptotic Expansion

The asymptotic expansion of $\tilde{Q}_{2D}(z)$ for small $|z|$ is given in Bernoff and Topaz (2011) for a strictly repulsion interaction,

$$\tilde{Q}_{2D}(z) = 2 + (\gamma - \frac{1}{2} - \ln 2)z^2 + z^2 \ln|z| + O(z^4 \ln|z).$$

When using the Morse potential we have both attraction and repulsion, so $Q_{2D}(z) = \tilde{Q}_{2D}(z) - C\tilde{Q}_{2D}(\frac{z}{L})$. Now we compute the asymptotic expansion of this for small value of $|z|$ by substituting the expression for the asymptotic expansion of $\tilde{Q}_{2D}$ above,

$$\begin{aligned}
Q_{2D}(z) &= \tilde{Q}_{2D}(z) - C\tilde{Q}_{2D}(\frac{z}{L}), \\
&= 2 + (\gamma - \frac{1}{2} - \ln 2)z^2 + z^2 \ln|z| - C(2 + (\gamma - \frac{1}{2} - \ln 2)\frac{z}{L}^2 + \frac{z}{L}^2 \ln|\frac{z}{L}|), \\
&= 2(1-C) + (1 - \frac{C}{L^2})(\gamma - \frac{1}{2} - \ln 2)z^2 + (1 - \frac{C}{L^2})z^2 \ln|z| + \frac{C}{L^2}\ln|L|, \\
&= 2(1-C) + \left[(1 - \frac{C}{L^2})(\gamma - \frac{1}{2} - \ln 2) + \frac{C}{L^2}\ln|L|\right] z^2 + (1 - \frac{C}{L^2})z^2 \ln|z|.
\end{aligned}$$

This is of the form $Q(z) = k + Az^2 + Bz^2 \ln|z|$, where $k = 2(1-C)$, $A = (1 - \frac{C}{L^2})(\gamma - \frac{1}{2} - \ln 2) + \frac{C}{L^2}\ln|L|$, and $B = (1 - \frac{C}{L^2})$. The constant $2(1-C)$ is a constant shift to the potential so this term can be disregarded. Thus, we can write $Q_{2D}(z)$ in the form

$$Q_{2D}(z) = Bz^2 \ln|ze^{\frac{A}{B}}|.$$

3.6 Carleman with the Morse Potential

Since the asymptotic expansion of the Morse Potential has the same form of the potential we solved Carleman's equation with, we can expect a solution of the form

$$\rho(y) = \frac{M}{\pi\sqrt{\ell^2 - y^2}}$$

for some value of ℓ. Here, we see that the value of the constant $k = \frac{M}{\pi}$ doesn't change since it only depended on the mass. Given the Morse potential function, we can compute what the length of the interval will be using this approximation. If we take two derivatives of the potential, we get $Q''(z) = 2A + B(2\log|z| + 3)$. Now we solve $\int \rho(y')Q(y-y')\mathrm{d}y' = \lambda$ in the same manner as before. We get

$$\begin{aligned}
\frac{d^2}{dy^2}\int_{-\ell}^{\ell}\rho(y')Q(y-y')\mathrm{d}y' &= \frac{d^2}{dy^2}\lambda,\\
\int_{-\ell}^{\ell}\rho(y')Q''(y-y')\mathrm{d}y' &= 0,\\
2B\int_{-\ell}^{\ell}\rho(y')\log|y-y'|\mathrm{d}y' + (3B+2A)\int_{-\ell}^{\ell}\rho(y')\mathrm{d}y' &= 0,\\
2B\int_{-\ell}^{\ell}\rho(y)\log|y-y'|\mathrm{d}y' + (3B+2A)M &= 0,\\
\int_{-\ell}^{\ell}\rho(y')\log|y-y'|\mathrm{d}y' = -M\frac{3B+2A}{2B} &= -M(\frac{3}{2}+\frac{A}{B}).
\end{aligned}$$

Now we use the result from the integral I in the previous section to compute the length scale,

$$\begin{aligned}
\frac{I}{C} &= \pi\log\ell - \pi\log 2,\\
-\pi(\frac{3}{2}+\frac{A}{B}) &= \pi\log\ell - \pi\log 2,\\
\log\ell &= -(\frac{3}{2}+\frac{A}{B}) + \log 2,\\
\ell &= 2e^{-(\frac{3}{2}+\frac{A}{B})}.
\end{aligned}$$

Next, we substitute in the value for A, B to solve for the length scale exactly,

$$\begin{aligned}
\frac{A}{B} &= \frac{(1-\frac{C}{L^2})(\gamma-\frac{1}{2}-\ln 2)+\frac{C}{L^2}\ln|L|}{(1-\frac{C}{L^2})},\\
\frac{A}{B} &= \gamma - \frac{1}{2} - \ln 2 + \frac{\frac{C}{L^2}\ln|L|}{\frac{L^2-C}{L^2}},\\
\frac{A}{B} &= \gamma - \frac{1}{2} - \ln 2 + \frac{C}{L^2-C}\ln|L|,\\
\frac{3}{2}+\frac{A}{B} &= \gamma + 1 - \ln 2 + \frac{C}{L^2-C}\ln|L|.
\end{aligned}$$

Substituting this above gives the length of the interval is

$$\ell = 4e^{-(\gamma+1)} L^{\frac{C}{C-L^2}}.$$

We wish to find for which values of C, L the analytic solution for Carleman's equation matches the numerical solution. Above we used the approximation that

$$Q(z) \approx 2(1-C) + \left[(1-\frac{C}{L^2})(\gamma - \frac{1}{2} - \ln 2) + \frac{C}{L^2}\ln|L|\right] z^2 + (1-\frac{C}{L^2}) z^2 \ln|z|.$$

This only holds for small values of $|z|$, so the analytic solution should only match for certain values of C, L when the asymptotic expansion of the potential is an accurate representation of the actual potential. For this to be the case, we want the zero of the asymptotic expansion to be close to 0. From Section 3.5, we saw that we could write

$$Q_{2D}(z) = Bz^2 \ln|ze^{\frac{A}{B}}|.$$

From this, we see that $Q_{2D}(z) = 0$ for $z = e^{-\frac{A}{B}}$. For this to occur close to the origin, we need for $\frac{A}{B} >> 1$.

$$\frac{A}{B} = \gamma - \frac{1}{2} - \ln 2 + \frac{C}{L^2 - C}\ln|L|.$$

In order for $\frac{A}{B} >> 1$; so we need for $C \approx L^2$, with the added condition that $C < L^2$. Thus we expect the analytic and numerical solution to be approximately equal near $C = L^2$. We compare how well the two solutions match by computing the width of the interval for the analytic and numeric solutions.

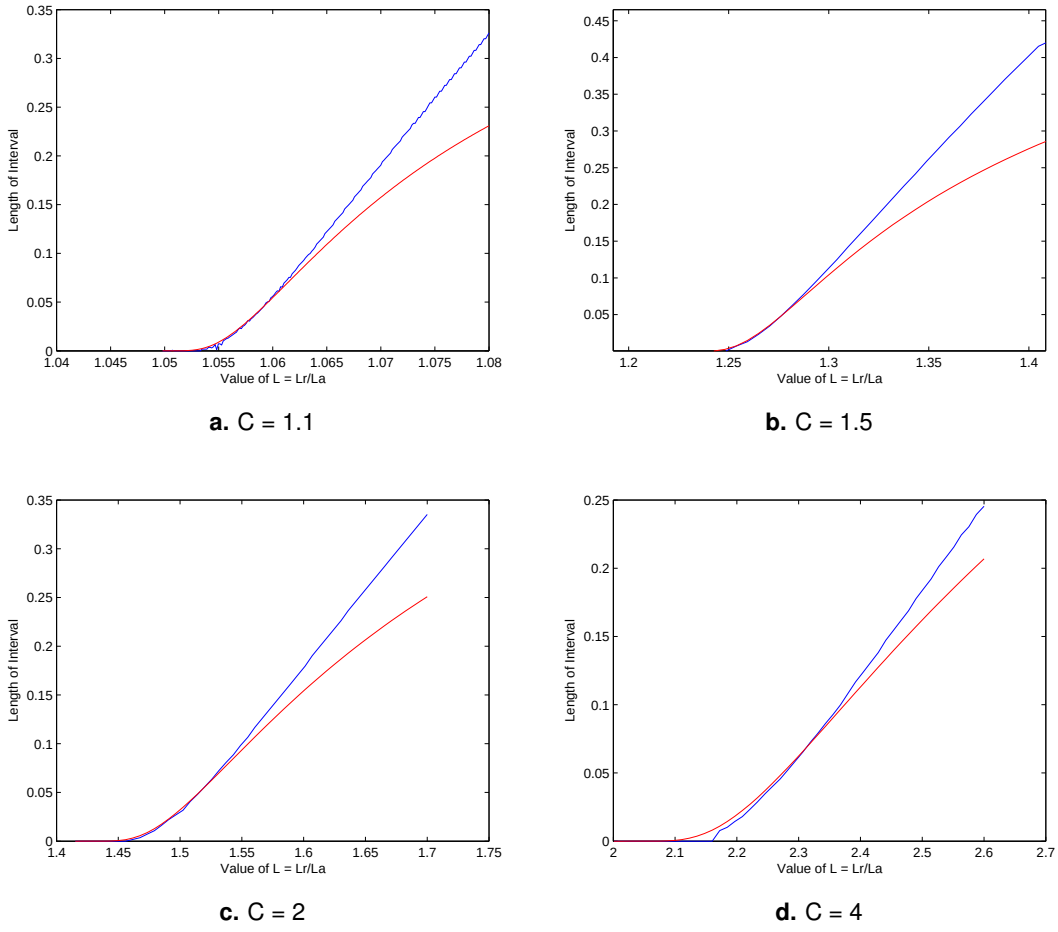

a. C = 1.1 **b.** C = 1.5

c. C = 2 **d.** C = 4

Figure 3.5 A comparison between Carleman's and the numerical solution as a function of L for 4 different values of C. The width of the interval predicted by Carleman's solution is in red and the numerical solution is in blue.

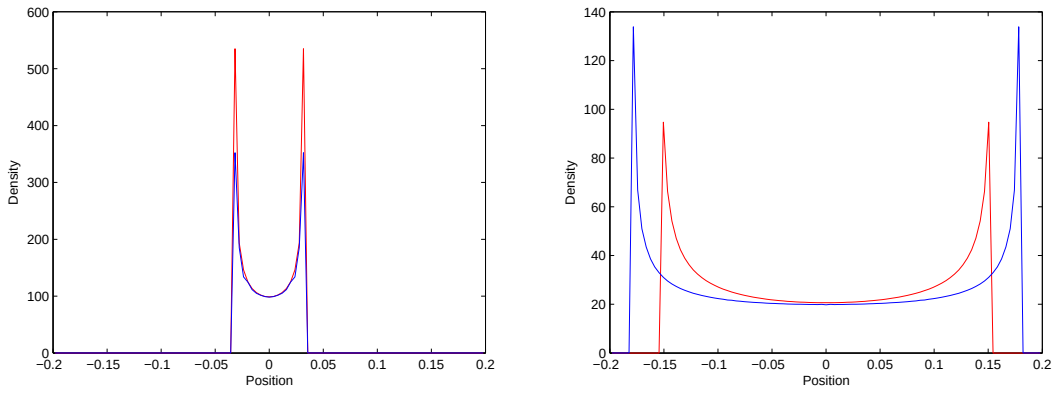

a. L = 1.5 **b.** L = 1.6

Figure 3.6 A comparison between Carleman's and the numerical solution as for $C = 2$, and $L = 1.5, 1.6$. Carleman's solution is in red and the numerical solution is in blue.

Chapter 4

Migration of a Circular Swarm

In this chapter we investigate the steady state solution of a migrating circular swarm. This steady state is frequently observed in the discrete model. In Section 2.2 we showed that a migrating circular swarm has the steady state solution $\rho = \rho(r), \mathbf{v} = \sqrt{\frac{\alpha}{\beta}}\hat{\mathbf{x}}$. This led to the integral equation,

$$\int_\Omega \rho(\mathbf{x}')Q(|\mathbf{x}-\mathbf{x}'|)\mathrm{d}\mathbf{x}' = \lambda,$$

where the domain $\Omega = r \in [0, R], \theta \in [0, 2\pi]$.

4.1 Energy Formulation

In order to solve this numerically, we use the same idea of minimizing an energy. The energy function needs to be modified so that a minimum is a solution to our integral equation,

$$\lambda = \rho * Q.$$

We start by rewriting the convolution,

$$\rho * Q = \int_{\mathbb{R}^2} \rho(\mathbf{y})Q(|\mathbf{x}-\mathbf{y}|)\, d\mathbf{y}.$$

Then we convert the integral to polar coordinates and replace $\rho(\mathbf{y}) = \rho(r)$ since the density is only a function of radius:

$$\rho * Q = \oint \int_{R=0}^{\infty} \rho(R)Q(|r-R|)R\, dR\, d\theta.$$

Here, $\oint d\theta$ indicates that the integral is taken from 0 to 2π. Now we define $\mu(r) = r\rho(r)$, which simplifies the above integral to

$$\rho * Q = \oint \int_{R=0}^{\infty} \mu(r) Q(|r - R|)\, dR\, d\theta.$$

Next, we apply the law of cosines,

$$|r - R| = \sqrt{r^2 + R^2 - 2rR\cos\theta},$$

and define the kernel function,

$$K(r, R) = \oint Q\left(\sqrt{r^2 + R^2 - 2rR\cos\theta}\right)\, d\theta.$$

We let the domain $\Omega = \{r : a < r < b\}$ be the support of ρ. This allows the above convolution to be written as

$$\rho * Q = \int_{\Omega} \mu(r) K(r, R)\, dR = \lambda.$$

Here the mass constraint is given by

$$M(\rho) \equiv \int_{\theta=0}^{2\pi} \int_{\Omega} \rho(r) r\, dr\, d\theta = \bar{M} = 2\pi \int_{\Omega} \mu(r)\, dr.$$

Using this formulation, we can now write this as a minimization problem to the energy function

$$W = \frac{1}{2} \int_{\Omega} \int_{\Omega} \mu(r)\mu(r') K(r, r')\, dr\, dr'.$$

When this is minimized subject to $M(\rho) = \bar{M}$ using the calculus of variations (Bernoff and Topaz, 2011), it yields

$$\lambda = \int_{\Omega} \mu(R) K(r, R)\, dR.$$

Thus, a minimization to this energy provides us with a solution for

$$\lambda = \rho * Q.$$

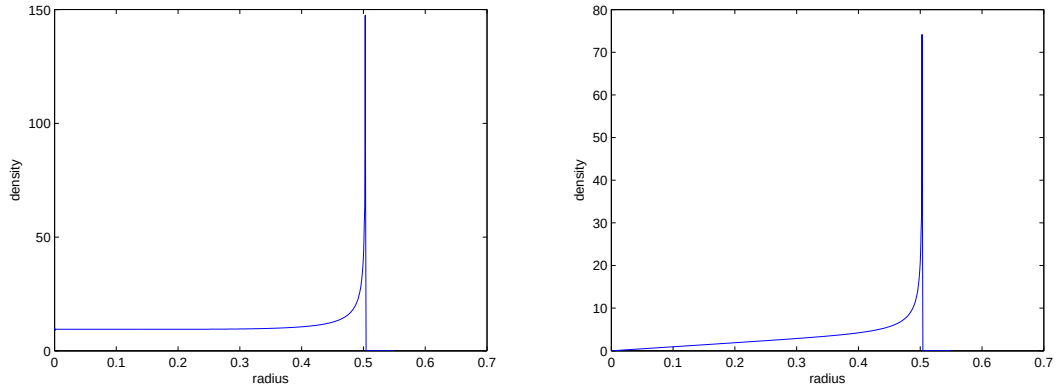

a. Swarm density $\rho(r)$ **b.** Swarm density $\mu(r)$

Figure 4.1 The swarm density $\rho(r)$ for a migrating circular swarm which contains a singularity. The plot on the right in the density $\mu(r)$ which is solved for by minimizing the energy. On the left is the actual density $\rho(r)$. This is for the parameter values C = 1.5 and L = 2.

4.2 Numerical Solution

Using this energy formulation, we can solve for a numerical solution of the density by using the same energy minimization technique as before. This provides a solution for $\mu(r) = r\rho(r)$. Thus, we compute the swarm density by taking

$$\rho(r) = \frac{\mu(r)}{r}.$$

The density for the circular swarm with parameter $C = 1.5$ and length scale $L = 2$ is given in Figure 4.1. In this numerical solution, we again notice a square root singularity occurring at the edge of the swarm. Locally, the swarm looks like an infinite ribbon for a particle near the boundary of the swarm. As a result, the same singularity observed on a ribbon occurs on a circular swarm.

4.3 Swarm Behavior

We are interested in the different types of steady state behaviors that we can observe. For biologically realistic potentials the value $L > 1$, so we focus our analysis to this regime. We investigate the different swarm behaviors

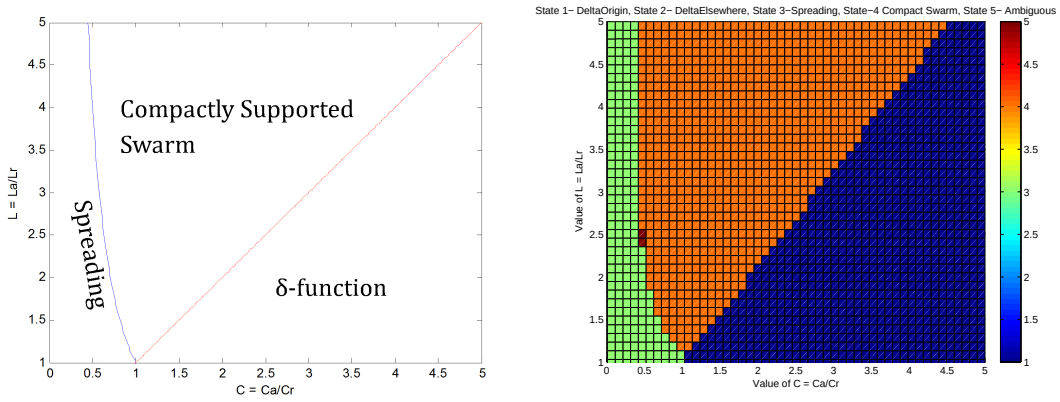

a. Analytic **b.** Numeric

Figure 4.2 A diagram determining the different regions of swarm behaviors for a migrating circular swarm. On the left is the analytic prediction for the regions and on the right is the numerical solution.

over a range of parameter values in this regime. The results are shown in Figure 4.2.

The behaviors that are observed are a delta function at the origin, a spreading swarm, and a compactly supported swarm. We would like to be able to quantify the parameters for which these behaviors are observed. We obtain when a delta function occurs from an expansion of the potential. Expanding $Q(z)$ gives

$$Q(z) = (1 - C) + (\frac{C}{L} - 1)|z| + O(z^2).$$

For $C > L$, the potential will have a local minimum at the origin. This implies that the solution $\rho(r)$ will contain a delta function at the origin for $C > L$, which matches our numerical results.

A spreading solution occurs when $E_\infty > 0$, where E_∞ is the potential

integrated over $\mathbb{R}^2$. Evaluating this gives

$$\begin{aligned}
E_\infty &= \oint \int_{r=0}^{\infty} Q(r) r \, dr \, d\theta, \\
&= 2\pi \int_{r=0}^{\infty} \left(e^{-r} - Ce^{-r/L} \right) r \, dr \, d\theta, \\
&= 2\pi r \left(-e^{-r} + CLe^{-r/L} \right) \Big|_{r=0}^{\infty} + 2\pi \int_{r=0}^{\infty} e^{-r} - CLe^{-r/L} \, dr \, d\theta, \\
&= 2\pi \left(-e^{-r} + CL^2 e^{-r/L} \right) \Big|_{r=0}^{\infty}, \\
&= 2\pi \left(1 - CL^2 \right).
\end{aligned}$$

For a spreading solution we require $E_\infty > 0$, so

$$1 - CL^2 > 0.$$

This implies that $C < \dfrac{1}{L^2}$ for a spreading solution which agrees with the numerical results.

Chapter 5

Milling Swarm

In this chapter we investigate the steady state solution of a milling swarm. A milling swarm is a swarm that rotates in a circle about its center. The mill is a common state observed in nature (Figure 1.2) and in the discrete model. In our previous Section 2.3,we showed that the steady state solution for a mill has the form $\rho = \rho(r), \mathbf{v} = \sqrt{\frac{\alpha}{\beta}}\hat{\theta}$. Analyzing this led to the integral equation

$$\int_\Omega \rho(\mathbf{x}')Q(|\mathbf{x}-\mathbf{x}'|)\mathrm{d}\mathbf{x}' = \sqrt{\frac{\alpha}{\beta}}\ln r + \lambda,$$

where we are on the circular domain $\Omega = r \in [a,b], \theta \in [0, 2\pi]$.

5.1 Energy Formulation

In order to solve this numerically, we use the same idea of minimizing an energy. The energy function needs to be modified so that a minimum is a solution to our integral equation,

$$\frac{\alpha}{\beta}\ln r + \lambda = \rho * Q.$$

We begin by proceeding in the same way as in the migrating circular swarm. After converting to radial coordinates we have

$$\rho * Q = \oint \int_{R=0}^{\infty} \rho(R)Q(|r-R|)R\,dR\,d\theta.$$

Now we define $\mu(r) = r\rho(r)$ and define the kernel function in the same way as before. After applying the law of cosines, we get

$$K(r, R) = \oint Q\left(\sqrt{r^2 + R^2 - 2rR\cos\theta}\right) d\theta.$$

We let the domain $\Omega = \{r : a < r < b\}$ be the support of ρ. We again have the mass constraint given by

$$M(\rho) \equiv \int_{\theta=0}^{2\pi} \int_{\Omega} \rho(r) r \, dr d\theta = \bar{M} = 2\pi \int_{\Omega} \mu(r) \, dr.$$

Using this formulation gives us the integral equation

$$\rho * Q = \int_{\Omega} \mu(r) K(r, R) \, dR = v_0 \ln r + \lambda,$$

where we let $v_0 = \dfrac{\alpha}{\beta}$. Here we have a function on the right side of the equation. To turn this into an energy minimization problem, we define the function

$$W = \frac{1}{2} \int_{\Omega}\int_{\Omega} \rho(r)\rho(r') K(r, r') \, dr \, dr' + \int_{\Omega} \rho(r) f(r) dr.$$

When this new energy functional is minimized subject to $M(\rho) = \bar{M}$ via calculus of variations (Bernoff and Topaz, 2011), it yields

$$-f(r) + \lambda = \int_{\Omega} \mu(r) K(r, R) \, dR.$$

Now if we let $f(r) = -\frac{\alpha}{\beta} \ln r$, then a minimization to this energy provides us with a solution for

$$\frac{\alpha}{\beta} \ln r + \lambda = \rho * Q.$$

5.2 Numerical Solution

Using this energy formulation, we solve for numerical solutions of the density using the same energy minimization technique as before. The only difference is the addition of the function $f(r) = -v_0 \ln r$. This function adds another parameter v_0 that we need to investigate. Using the energy minimization method provides us with a solution for $\mu(r) = r\rho(r)$, so we obtain the actual density $\rho(r) = \dfrac{\mu(r)}{r}$.

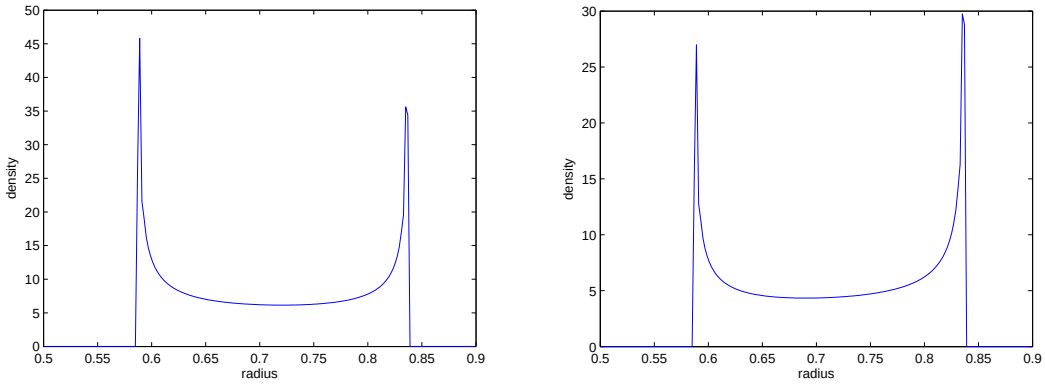

a. Swarm density $\rho(r)$ **b.** Swarm density $\mu(r)$

Figure 5.1 The swarm density for milling solutions for the parameter values $C = 1.2$ and $L = 1.5$. Here, $\mu(r)$ is solved for by minimizing the energy. On the left is the actual density $\rho(r)$.

We again observe singularities on the boundary of the swarm for a swarm with compact support. From a Lagrangian point of view, the milling swarm looks like the infinite strip. Therefore, we expect the density to be similar to that of the infinite strip with square root singularities on the boundary.

5.3 Swarm Behavior

The addition of a velocity parameter v_0 creates a three-dimensional parameter space to investigate. We investigate this for different fixed values of C, L to determine the different swarm behaviors. Since the potential $Q(z)$ here is the same as the potential used for the migrating circular swarm, we still get a minimum in the potential for $C > L$. This implies that the density $\mu(r)$ will be a delta function for $C > L$. Also, we know that a spreading solution will occur for $C < \frac{1}{L^2}$. The analytical phase diagram is identical to the one observed in the migrating circular swarm in Figure 4.2. These constraints match our numerical solutions for the behavior seen in Figures 5.2 and 5.3.

When we examine the swarm behaviors in the milling case, we notice that a new solution of a delta function away from the origin exists. This oc-

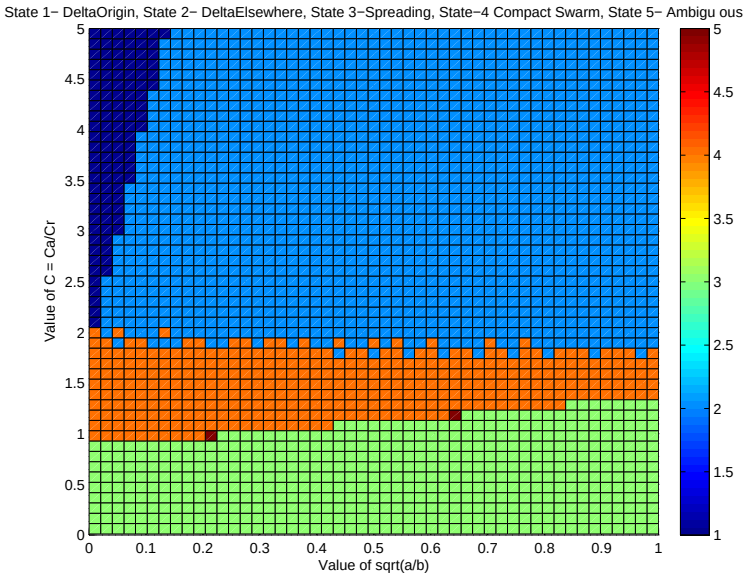

Figure 5.2 A diagram determining the different regions of swarm behaviors for a milling swarm. Here we are holding $L = 2$ fixed and investigating over parameter ranges for v_0 and C.

curs because the milling solution has a centripetal force that pushes the particles outwards. Mathematically, this is the forcing function $v_0 \ln r$ which shifts the radius where the minimum energy density occurs.

Near the boundary where $C = L$, we notice a transition from a delta function to a compactly supported swarm. The width of the compactly supported swarm will be very small near this boundary so we expect for Carleman's approximation to hold near this boundary. We would like to find a region where Carleman's solution agrees with the numerical solution. In order to do this, we must first investigate how the swarm behaves on the boundary $C = L$ to determine how the ring radius is affected by the parameters in our model.

5.4 Solutions on the Boundary C = L

Here we are looking for solutions on the boundary where $C = L$. Our potential function Q is given by

$$\begin{aligned} Q(z) &= e^{-|z|} - Ce^{-|z|/L}, \\ &= e^{-|z|} - Le^{-|z|/L}. \end{aligned}$$

Next, an asymptotic expansion of the potential is performed in the same manner as in the Ribbon Chapter 3. This gives the quadratic potential

$$Q(z) = (1 - L) + \frac{L-1}{2L} z^2 + O(z^3).$$

Let $A = \frac{(L-1)}{2L}$. Since a quadratic potential allows for the kernel to be computed analytically, we can compute

$$\begin{aligned} K(r, r') &= \oint Q\left(\sqrt{r^2 + r'^2 - 2rr'\cos\theta}\right)\, d\theta \\ &= \oint (1 - L) + \frac{L-1}{2L^2}\left(r^2 + r'^2 - 2rr'\cos\theta\right)\, d\theta, \end{aligned}$$

which yields

$$K(r, r') = 2\pi(1 - L) + 2\pi A(r^2 + r'^2).$$

Now let the parameter $v_0 = \alpha/\beta$. Substituting this into the energy functional

$$W = \frac{1}{2}\int_\Omega\int_\Omega \mu(r)\mu(r')K(r, r')\, dr\, dr' + \int_\Omega \mu(r) f(r) dr,$$

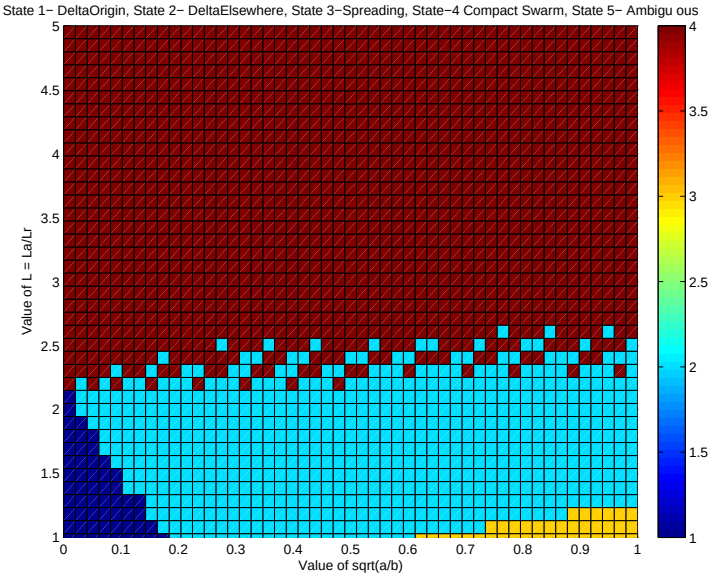

a. Fixed $C = 2$

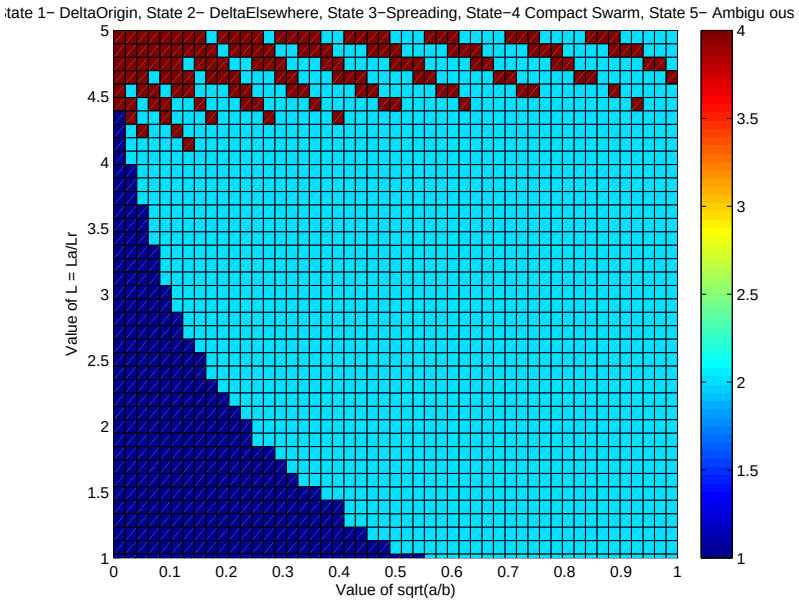

b. Fixed $C = 4$

Figure 5.3 A diagram determining the different regions of swarm behaviors for a milling swarm. Here we hold C fixed and investigating over parameter ranges for v_0 and L.

and evaluating this yields

$$\begin{aligned} W &= \frac{1}{2}\int_\Omega\int_\Omega \mu(r)\mu(r')\left(2\pi(1-L)+\pi\frac{L-1}{L}(r^2+r'^2)\right)\,dr\,dr' - v_0\int_\Omega \mu(r)\ln r dr, \\ &= \pi(1-L)\frac{M}{2\pi}^2 + AM\int_\Omega \mu(r)r^2\,dr - v_0\int_\Omega \mu(r)\ln r\,dr, \\ &= \pi(1-L)\frac{M}{2\pi}^2 + AM\int_\Omega \mu(r)\left(r^2-\frac{v_0}{AM}\ln r\right)\,dr. \end{aligned}$$

Since we are trying to minimize the potential, the addition of any constant term will have no effect on the solution. We let $W_0 = \pi(1-L)\frac{M}{2\pi}^2$ and define $2R^2 = \frac{v_0}{AM}$. This simplifies our potential to

$$W = W_0 + AM\int_\Omega \mu(r)\left(r^2 - 2R^2\ln r\right)\,dr. \tag{5.1}$$

Now define the function $g(r) = r^2 - 2R^2\ln r$ and expand this around $r = R$. Evaluating the first and second derivative yields $g'(r) = 2r - 2R^2/r$ and $g''(r) = 2 + 2R^2/r^2$. This gives the expansion

$$g(R+\sigma) = (R^2 - 2R^2\ln R) + 2\sigma^2 + O(\sigma^3).$$

Substituting this into the energy above gives

$$W = \tilde{W}_0 + 2AM\int_\Omega \mu(R+\sigma)\sigma^2\,d\sigma.$$

Any perturbation to a delta function at $r = R$ causes an increase in energy. Therefore, the density for this must follow $\mu(r) = M\delta(r-R)$, where the radius

$$R = \sqrt{\frac{v_0}{2AM}} = \sqrt{\frac{v_0 L}{M(L-1)}}. \tag{5.2}$$

We investigate whether the delta function is stable numerically for this case. The energy for a delta function $\mu(r) = \frac{M}{2\pi}\delta(r-R)$ is given by

$$W = \frac{1}{2}\frac{M}{2\pi}^2 K(R,R) - \frac{M}{2\pi}v_0\ln r.$$

We compute the energy numerically for this and perturbations to this to confirm that this is indeed a minimum for the energy. From Figure 5.4, we see that a delta function is stable on the boundary where $C = L$.

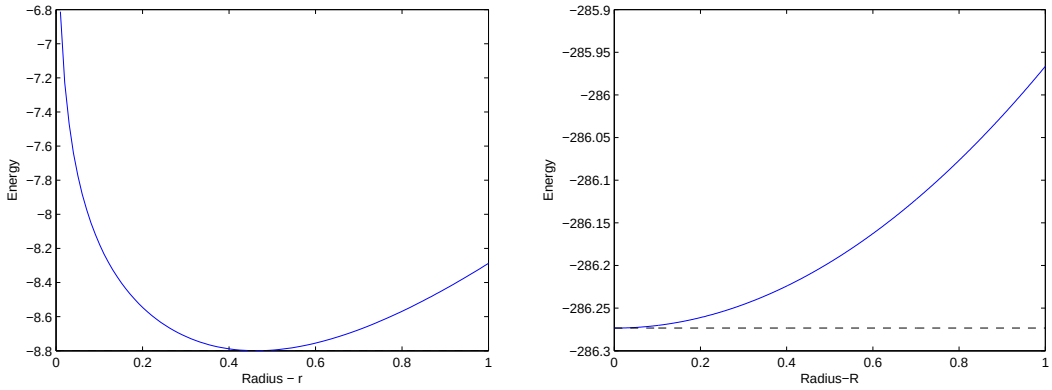

a. Energy Density **b.** Energy

Figure 5.4 The left graph shows the energy density as a function of the radius from the origin. On the right is the energy as a function of ϵ where ϵ represents a solution $\mu(r)$ to be a top hat function of width ϵ centered at $r = 0.47$. This is for the parameter values $C = L = 2$, $M = 10$, and $v_0 = 0.6$.

Next, we investigate how well the actual radius of the ring matches the value predicted by the asymptotic expansion of the potential. The asymptotic expansion of $Q(z)$ is a good approximation for small values of z. Therefore, we expect the radius of the ring to match the predicted value of R for small R. This means we want $v_0 = \alpha/\beta$ to be small, or the mass M to be large. A comparison between the numerical and predicted value from the asymptotic expansion is shown in Figure 5.4. We observe that the approximation works well for small v_0 or large M as expected.

5.5 Carleman with the Morse Potential

Now we consider the behavior of the swarm as we move slightly from the boundary. We consider the case when $C = L - \epsilon$. An asymptotic expansion of the potential gives

$$Q(z) = (1 - L + \epsilon) - \frac{\epsilon}{L}|z| + \frac{L^2 - L + \epsilon}{2L^2}z^2 + O(z^3).$$

We will let $A = \frac{L^2-L+\epsilon}{2L^2}$ and $B = \frac{-\epsilon}{L}$. Define $Q_0 = B|z|$ and $Q_1 = Az^2$. Then we have the kernel, $K = K_0 + K_1$. From above, we already know the effect

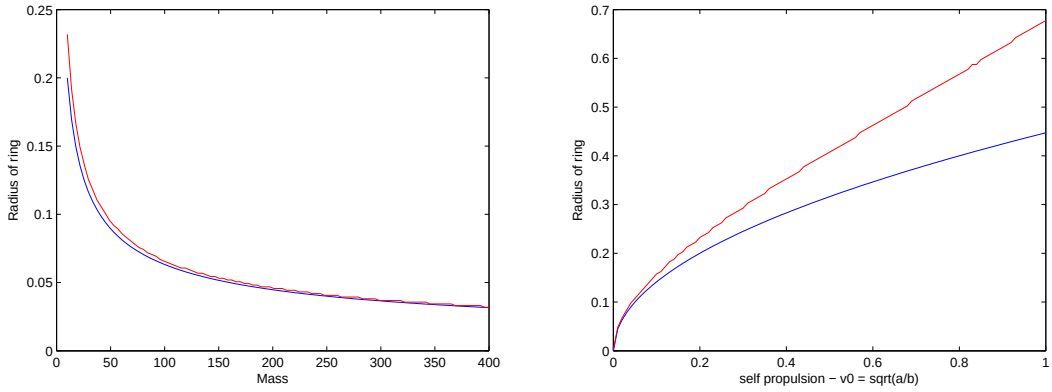

a. Effect of Mass **b.** Effect of v_0

Figure 5.5 A comparison between numerical ring radius in red and the asymptotic result in blue as functions of M and v_0. The left plot shows the effect that the mass has on the ring radius R. The right plot shows the effect of v_0 on the ring radius. This is for the parameter values $C = L = 2$, $M = 10$, and $v_0 = 0.5$.

of the kernel K_1 on the energy. Therefore, all that is left is to evaluate K_0. Computing the integral gives

$$K_0(r,r') = \oint Q_0\left(\sqrt{r^2 + r'^2 - 2rr'\cos\theta}\right) d\theta = B\oint \sqrt{r^2 + r'^2 - 2rr'\cos\theta}\, d\theta,$$

which yields

$$K_0(r,r') = 4B(r+r')\text{EllipticE}\left(\frac{2\sqrt{rr'}}{r+r'}\right).$$

Now let $r = R + \sigma_1$ and $r' = R + \sigma_2$ where we assume $\sigma_1, \sigma_2 << 1$ and $R = \sqrt{\dfrac{v_0}{2AM}}$ is given by Equation 5.2. An asymptotic expansion of the kernel K_0 under these conditions gives

$$K_0 = 8RB + 4B(\sigma_1 + \sigma_2) + B\frac{|\sigma_1 - \sigma_2|^2}{R}(2\ln 8R - 1 - \ln|\sigma_1 - \sigma_2|).$$

Combining the terms into one log gives

$$K_0 = 8RB + 4B(\sigma_1 + \sigma_2) - B\frac{|\sigma_1 - \sigma_2|^2}{R}\ln\frac{\sqrt{e}}{8R}|\sigma_1 - \sigma_2|.$$

Now we evaluate the effect of the energy from this kernel after defining $C = \frac{\sqrt{e}}{8R}$. The new effect comes from $W_\epsilon = \frac{1}{2}\int_\Omega\int_\Omega \mu(r)\mu(r')K_0(r,r')\,dr\,dr'$. Evaluating this gives

$$\begin{aligned}
W_\epsilon &= \frac{1}{2}\int_\Omega\int_\Omega \mu(R+\sigma_1)\mu(R+\sigma_2)K_0(\sigma_1,\sigma_2)\,d\sigma_1\,d\sigma_2,\\
&= \frac{1}{2}\int_\Omega\int_\Omega \mu(R+\sigma_1)\mu(R+\sigma_2)\left(8RB + 4B(\sigma_1+\sigma_2) - B\frac{|\sigma_1-\sigma_2|^2}{R}\ln C|\sigma_1-\sigma_2|\right)\,d\sigma_1\,d\sigma_2,\\
&= 4RB\frac{M}{2\pi}^2 + 4B\frac{M}{2\pi}\int_\Omega \mu(R+\sigma)\sigma\,d\sigma,\\
&\quad - \frac{B}{2}\int_\Omega\int_\Omega \mu(R+\sigma_1)\mu(R+\sigma_2)\left(\frac{|\sigma_1-\sigma_2|^2}{R}\ln C|\sigma_1-\sigma_2|\right)\,d\sigma_1\,d\sigma_2.
\end{aligned}$$

Next we combine this with the energy for the kernel K_1 given in Equation 5.1 where $r = R+\sigma$. All of the constants are combined into a single constant W_0, which yields

$$\begin{aligned}
W = W_0 + \int_\Omega \mu(R+\sigma)\left[\left(AM(R+\sigma)^2 - 2R^2\ln(R+\sigma)\right) + 2\frac{B}{\pi}M\sigma\right]\,d\sigma -\\
\frac{B}{2R}\int_\Omega\int_\Omega \mu(R+\sigma_1)\mu(R+\sigma_2)\left(|\sigma_1-\sigma_2|\ln C|\sigma_1-\sigma_2|\right)\,d\sigma_1\,d\sigma_2.
\end{aligned}$$

When this is minimized subject to $M(\mu) = \bar{M}$ using the calculus of variations, it yields

$$\left[AM(R+\sigma)^2 - 2R^2\ln(R+\sigma)\right] + 2\frac{B}{\pi}M\sigma + \tilde{\lambda} = \frac{B}{R}\int_\Omega \mu(R+\sigma_1)\left(|\sigma_1-\sigma|^2\ln C|\sigma_1-\sigma|\right)\,d\sigma_1.$$

This can be written in terms of r as

$$\left[AMr^2 - 2R^2\ln r\right] + 2\frac{B}{\pi}M(r-R) + \tilde{\lambda} = \frac{B}{R}\int_\Omega \mu(r)\left(|r_1-r|^2\ln C|r_1-r|\right)\,dr_1.$$

This leads to an integral equation in a similar form as Carleman's equation which we solved earlier. However, the linear term $2\frac{B}{\pi}M\sigma$ causes a shift in the center of the swarm. We define the left hand side as a function $f(r)$, and find the minimum of this to determine the center of the swarm,

$$f(r) = AM(r^2 - 2R^2\ln r) + 2\frac{B}{\pi}M(r-R). \tag{5.3}$$

Differentiating to find where the derivative is 0 yields

$$f'(r) = 2AM(r - R^2\frac{1}{r}) + 2\frac{B}{\pi}M = 0.$$

Simplifying the above result into a quadratic gives

$$r^2 + \frac{B}{\pi A} r - R^2 = 0.$$

Solving this using the quadratic formula gives

$$r_\epsilon = \frac{-\frac{B}{\pi A} + \sqrt{(\frac{B}{\pi A})^2 + 4R^2}}{2}.$$

We define $\tilde{\epsilon} = \frac{B}{2\pi A}$ which allows us to simplify the above result to

$$r_\epsilon = \sqrt{\tilde{\epsilon}^2 + R^2} - \tilde{\epsilon}.$$

Thus, we expect to have a solution symmetric about the point r_ϵ. We will now let $\sigma = r - r_\epsilon$ which we use to solve Carleman's equation. Therefore, we can expect a solution of the form

$$\tilde{\mu}(\sigma) = \frac{k}{\sqrt{\ell^2 - \sigma^2}}$$

for some value of k, ℓ.

We can compute what the length of the interval will be using this approximation. If we take two derivatives of the potential $\tilde{Q} = |\sigma_1 - \sigma'|^2 \ln C|\sigma_1 - \sigma'|$ we get

$$Q''(z) = 2\ln C + 2\log|z| + 3.$$

Now we solve Carleman's equation as we did in the ribbon chapter.

$$\frac{B}{R}\frac{d^2}{d\sigma^2}\int_{-\ell}^{\ell} \tilde{\mu}(\sigma_1) Q(\sigma - \sigma_1) \mathrm{d}\sigma_1 = \frac{d^2}{d\sigma^2} f(r_\epsilon),$$
$$\frac{B}{R}\int_{-\ell}^{\ell} \tilde{\mu}(\sigma_1) Q''(\sigma - \sigma_1) \mathrm{d}\sigma_1 = f''(r_\epsilon).$$

Note that $\dfrac{d}{d\sigma} = \dfrac{d}{dr}$ so we will compute $\frac{d^2}{dr^2}$ of the function $f(r)$ given in Equation 5.3. This gives

$$f''(r) = 2AM(1 + R^2\frac{1}{r^2}).$$

This is evaluated at $r = r_\epsilon$ which gives

$$f''(r_\epsilon) = 2AM[1 + (\frac{R}{r_\epsilon})^2].$$

Substituting this in above yields

$$\frac{2B}{R}\int_{-\ell}^{\ell}\tilde{\mu}(\sigma_1)\log|\sigma-\sigma_1|\mathrm{d}\sigma_1+\frac{B}{R}(3+2\ln C)\int_{-\ell}^{\ell}\tilde{\mu}(\sigma_1)\mathrm{d}\sigma_1=2AM\left[1+\left(\frac{R}{r_\epsilon}\right)^2\right],$$

$$\frac{2B}{R}\int_{-\ell}^{\ell}\tilde{\mu}(\sigma_1)\log|\sigma-\sigma_1|\mathrm{d}\sigma_1+\frac{B}{R}\frac{(3+2\ln C)M}{2\pi}=2AM\left[1+\left(\frac{R}{r_\epsilon}\right)^2\right],$$

$$\int_{-\ell}^{\ell}\tilde{\mu}(\sigma_1)\log|\sigma-\sigma_1|\mathrm{d}\sigma_1=\frac{AMR}{B}\left(1+\frac{R}{r_\epsilon}^2\right)-\frac{M(3+2\ln C)}{4\pi}.$$

The mass constraint is used to compute the value of the constant k,

$$\begin{aligned}\frac{M}{2\pi}&=\int_{-\ell}^{\ell}\mu(\sigma)\mathrm{d}\sigma,\\&=\int_{-\ell}^{\ell}\frac{k}{\sqrt{\ell^2-\sigma^2}}\mathrm{d}\sigma,\\&=k\pi,\\k&=\frac{M}{2\pi^2}.\end{aligned}$$

Now we use the result for the integral $I/k=\int_{-\ell}^{\ell}\tilde{\mu}(\sigma_1)\log|\sigma_1-\sigma|\mathrm{d}\sigma$ from Section 3.4 to compute the length scale,

$$\begin{aligned}\frac{I}{k}&=\pi\log\ell-\pi\log 2,\\\frac{2\pi^2}{M}\left(\frac{AMR}{B}\left[1+\frac{R}{r_\epsilon}^2\right]-\frac{M(3+2\ln C)}{4\pi}\right)&=\pi\log\ell-\pi\log 2.\end{aligned}$$

This gives the length scale for the interval,

$$\begin{aligned}\log\ell&=\frac{2\pi AR}{B}\left(1+\frac{R}{r_\epsilon}^2\right)-\frac{3+2\ln C}{2}+\log 2,\\\ell&=2\mathrm{Exp}\left[\frac{2\pi AR}{B}\left(1+\frac{R}{r_\epsilon}^2\right)-\frac{3+2\ln C}{2}\right],\end{aligned}\tag{5.4}$$

where $A=\dfrac{L^2-L+\epsilon}{2L^2}$, $B=\dfrac{-\epsilon}{L}$, and $C=\dfrac{\sqrt{e}}{8R}$.

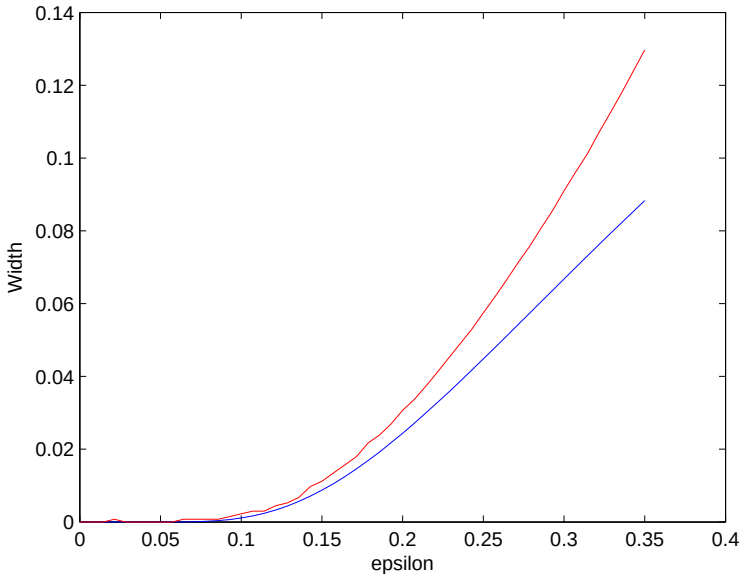

Figure 5.6 The width of the solution as a function of ϵ as we move in from the boundary $C = L$. The numerical solution using the Morse potential is in red and the analytical solution using an asymptotic approximation is in blue. This is for the parameters $C = L = 2$, $M = 100$, and $v_0 = 0.5$.

Hence, our solution to this integral equation is given by

$$\mu(r) = \frac{M}{2\pi^2\sqrt{\ell^2 - (r - r_\epsilon)^2}},$$

where ℓ is given above in Equation 5.4. The width of the interval is given by $w = 2\ell$. We compare how good an approximation this is for the solution in Figure 5.6.

Chapter 6

Conclusion

In this thesis, we investigated the different steady state behaviors that can exist in our swarming model. Our model for the swarms behavior used a nonlocal PDE to model the social interactions that occur between individuals. We studied the Morse potential since it has been used for a long period of time to model social interactions between individuals (Levine et al., 2000).

The three steady states we investigated were an infinite ribbon, a migrating circular swarm, and a milling swarm. Both the migrating circular swarm and milling swarm are behaviors exhibited by animals in nature. The infinite ribbon provided a way to determine an analytic solution for the singularity. Using an asymptotic expansion of the potential we were able to convert our integral equation into Carleman's equation, which can be solve analytically. Locally, the milling swarm as well as the boundary of the migrating circular swarm can be thought of as an infinite ribbon. This leads to the same square root singularity that was observed in the infinite ribbon.

Our results indicate that the use of the Morse potential for social interactions leads to a singularity in the swarm density. However, the Morse potential is being used to model a biological process where an infinite density of animals is unrealistic. This calls into question the validity of the Morse potential for swarming models and suggests that a different potential should be used instead to model the social interactions that occur between individuals.

Chapter 7

Future Direction

In the ribbon and milling steady states, we found an analytic solution for the asymptotic expansion of the potential. This matched with the numerical solution to the integral equation for a specific range of parameters. The range of parameters over which the analytic solution is accurate could be extended by using more terms in the asymptotic expansion of the potential.

In our investigation, we used an energy minimization technique to obtain the solution for the density. However, we do not know whether this results is a local or global minimum for the different solutions we observe. Therefore, we would like to perform stability analysis on the steady states. This can be done by investigating the effects of small perturbations on the solution to determine their stability.

Our analysis focused on swarm behavior in two dimensions. We found both a mill and a migrating steady state which are both biological behaviors. Future work could extend this by investigating the steady states that exist in three dimensions. This might provide insight into the types of behaviors observed in birds. Also, three dimensions allows for the addition of new steady states such as helixes.

Bibliography

Ballerini, M., N. Cabibbo, R. Candelier, A. Cavagna, E. Cisbani, I. Giardina, V. Lecomte, A. Orlandi, G. Parisi, A. Procaccini, M. Viale, and V. Zdravkovic. 2008. Interaction ruling animal collective behavior depends on topological rather than metric distance: Evidence from a field study. *Proceedings of the National Academy of Sciences* 105(4):1232–1237. doi:10.1073/pnas.0711437105.

Becco, C., N. Vandewalle, J. Delcourt, and P. Poncin. 2006. Experimental evidences of a structural and dynamical transition in fish school. *Physica A: Statistical Mechanics and its Applications* 367:487–493.

Bernoff, A.J., and C.M. Topaz. 2011. A primer of swarm equilibria. *SIAM Journal on Applied Dynamical Systems* 10(1):212–250.

Bumann, Dirk, Jens Krause, and Dan Rubenstein. 1997. Mortality risk of spatial positions in animal groups: The danger of being in the front. *Behaviour* 134(13/14):pp. 1063–1076.

Chuang, Y., M.R. D'Orsogna, D. Marthaler, A.L. Bertozzi, and L.S. Chayes. 2007. State transitions and the continuum limit for a 2D interacting, self-propelled particle system. *Physica D: Nonlinear Phenomena* 232(1):33–47.

Couzin, Iain D., Jens Krause, Richard James, Graeme D. Ruxton, and Nigel R. Franks. 2002. Collective memory and spatial sorting in animal groups. *Journal of Theoretical Biology* 218(1):1 – 11. doi:DOI: 10.1006/jtbi.2002.3065.

Couzin, I.D., and J. Krause. 2003. Self-organization and collective behavior in vertebrates. *Advances in the Study of Behavior* 32:1–75.

Couzin, I.D., J. Krause, N.R. Franks, and S.A. Levin. 2005. Effective leadership and decision-making in animal groups on the move. *Nature: International Weekly Journal of Science* .

D'Orsogna, M.R., Y.L. Chuang, A.L. Bertozzi, and L.S. Chayes. 2006. Self-propelled particles with soft-core interactions: Patterns, stability, and collapse. *Phys Rev Lett* 96(10):104,302. doi:10.1103/PhysRevLett.96.104302.

Eriksson, Anders, Martin Nilsson Jacobi, Johan Nyström, and Kolbjørn Tunstrøm. 2010. Determining interaction rules in animal swarms. *Behavioral Ecology* 21(5):1106–1111. doi:10.1093/beheco/arq118.

Gueron, S., S.A. Levin, and D.I. Rubenstein. 1996. The dynamics of herds: From individuals to aggregations. *Journal of Theoretical Biology* 182(1):85–98.

Hall, S.J., C.S. Wardle, and D.N. MacLennan. 1986. Predator evasion in a fish school: Test of a model for the fountain effect. *Marine Biology* 91(1):143–148.

Hamilton, W.D. 1971. Geometry for the selfish herd. *Journal of Theoretical Biology* 31(2):295–311.

Hannant, M. 2009. Blacktip reef sharks in huge shoal of fish at Kuredu Maldives. online; last viewed 03 May 2012. URL http://www.youtube.com/watch?v=KasJjuuaCiM.

Hemelrijk, C.K., and H. Kunz. 2005. Density distribution and size sorting in fish schools: An individual-based model. *Behavioral Ecology* 16(1):178.

Holmes, E.E., M.A. Lewis, J.E. Banks, and R.R. Veit. 1994. Partial differential equations in ecology: Spatial interactions and population dynamics. *Ecology* 75(1):17–29.

Lee, S.-H., H.K. Pak, and T.-S. Chon. 2006. Dynamics of prey-flock escaping behavior in response to predator's attack. *Journal of Theoretical Biology* 240(2):250 – 259. doi:DOI: 10.1016/j.jtbi.2005.09.009.

Leverentz, A., C.M. Topaz, and A.J. Bernoff. 2009. Asymptotic dynamics of attractive-repulsive swarms. *SIAM Journal on Applied Dynamical Systems* 8(3):880–908.

Levine, H., W.J. Rappel, and I. Cohen. 2000. Self-organization in systems of self-propelled particles. *Physical Review E* 63(1):017,101.

Lukeman, Ryan, Yue-Xian Li, and Leah Edelstein-Keshet. 2010. Inferring individual rules from collective behavior. *Proceedings of the National Academy of Sciences* 107(28):12,576–12,580. doi:10.1073/pnas.1001763107.

McInnes, C.R. 2007. Vortex formation in swarms of interacting particles. *Physical Review E* 75(3):032,904.

Mecholsky, Nicholas A., Edward Ott, and Thomas M. Antonsen, Jr. 2010. Obstacle and predator avoidance in a model for flocking. *Physica D-Nonlinear Phenomena* 239(12):988–996. doi:10.1016/j.physd.2010.02.007.

Mogilner, A., L. Edelstein-Keshet, L. Bent, and A. Spiros. 2003. Mutual interactions, potentials, and individual distance in a social aggregation. *Journal of Mathematical Biology* 47(4):353–389.

Mogilner, Alexander, and Leah Edelstein-Keshet. 1999. A non-local model for a swarm. *Journal of Mathematical Biology* 38:534–570. 10.1007/s002850050158.

Romey, W.L. 1996. Individual differences make a difference in the trajectories of simulated schools of fish. *Ecological Modelling* 92(1):65–77.

Romey, W.L., and A.C. Wallace. 2007. Sex and the selfish herd: Sexual segregation within nonmating whirligig groups. *Behavioral Ecology* 18(5):910.

Sumpter, D.J.T. 2010. *Collective Animal Behavior*. Princeton Univ Pr.

Swain, D.T., I.D. Couzin, and N. Ehrich Leonard. 2011. Real-time feedback-controlled robotic fish for behavioral experiments with fish schools. *Proceedings of the IEEE* 100(99):1–14.

Takagi, T., Y. Moritomi, J. Iwata, H. Nakamine, and N. Sannomiya. 2004. Mathematical model of fish schooling behaviour in a set-net. *ICES Journal of Marine Science: Journal du Conseil* 61(7):1214.

Tang, W.J., Q.H. Wu, and J.R. Saunders. 2007. A bacterial swarming algorithm for global optimization. In *Evolutionary Computation, 2007. CEC 2007. IEEE Congress on*, 1207–1212. IEEE.

Tien, J.H., S.A. Levin, and D.I. Rubenstein. 2004. Dynamics of fish shoals: Identifying key decision rules. *Evolutionary Ecology Research* 6(4):555–565.

Vicsek, T., and A. Zafiris. 2010. Collective motion. *ArXiv e-prints* .

Viscido, Steven V., Julia K. Parrish, and Daniel Grunbaum. 2007. Factors influencing the structure and maintenance of fish schools. *Ecological Modelling* 206(1-2):153 – 165. doi:DOI: 10.1016/j.ecolmodel.2007.03.042.

Viscido, S.V., and D.S. Wethey. 2002. Quantitative analysis of fiddler crab flock movement: Evidence for selfish herd behaviour. *Animal Behaviour* 63(4):735–741.

Ward, A.J.W., D.J. Hoare, I.D. Couzin, M. Broom, and J. Krause. 2002. The effects of parasitism and body length on positioning within wild fish shoals. *Journal of Animal Ecology* 71(1):10–14.

Wood, Andrew J., and Graeme J. Ackland. 2007. Evolving the selfish herd: Emergence of distinct aggregating strategies in an individual-based model. *Proceedings of the Royal Society B: Biological Sciences* 274(1618):1637–1642. doi:10.1098/rspb.2007.0306.

Zhdankin, Vladimir, and J.C. Sprott. 2010. Simple predator-prey swarming model. *Physical Review E* 82(5, Part 2). doi:10.1103/PhysRevE.82.056209.

Zheng, M., Y. Kashimori, O. Hoshino, K. Fujita, and T. Kambara. 2005. Behavior pattern (innate action) of individuals in fish schools generating efficient collective evasion from predation. *Journal of Theoretical Biology* 235(2):153–167.